Evaluation of Mei-yu Heavy-Rainfall Quantitative Precipitation Forecasts in Taiwan by A Cloud-Resolving Model for Three Seasons of 2012-2014

Chung-Chieh Wang[1], Pi-Yu Chuang[1]*, Chih-Sheng Chang[1], Kazuhisa Tsuboki[2], Shin-Yi Huang[1], and Guo-Chen Leu[3]

1 Department of Earth Sciences, National Taiwan Normal University, Taipei, Taiwan
2 Institute for Space-Earth Environmental Research, Nagoya University, Nagoya, Japan
3 Central Weather Bureau, Taipei, Taiwan

Corresponding author: Pi-Yu Chuang (giselle780507@hotmail.com)

Abstract.

In this study, the performance of quantitative precipitation forecasts (QPFs) by the Cloud-Resolving Storm Simulator (CReSS) in Taiwan, at a horizontal grid spacing of 2.5 km and a domain size of 1500 × 1200 km^2, at the ranges of 1-3 days during three mei-yu seasons (May-June) of 2012-2014 is evaluated using categorical statistics, with an emphasis on heavy rainfall events (≥ 100 mm per 24 h). The categorical statistics are chosen because the main hazards are landslides and floods in Taiwan, so predicting heavy rainfall at the correct location is important. The overall threat scores (TSs) of QPFs for all events on day 1 (0-24 h) are 0.18, 0.15, and 0.09 at the threshold of 100, 250, and 500 mm, respectively, and indicate considerable improvements at increased resolution compared to past results and 5-km models.

Moreover, the TSs are shown to be higher and the model more skillful in predicting larger events, in agreement with earlier findings for typhoons. After classification based on observed rainfall, the TSs of day-1 QPFs for the largest 4% of events by CReSS at 100, 250, and 500 mm (per 24 h) are 0.34, 0.24, and 0.16, respectively, and can reach 0.15 at 250 mm on day 2 (24-48 h) and 130 mm on day 3 (48-72 h). The larger events also exhibit higher probability of detection and lower false alarm ratio than smaller ones almost without exception across all thresholds. With the convection and terrain better resolved, the strength of the model is found to lie mainly in the topographic rainfall in Taiwan rather than migratory events that are more difficult to predict. Our results highlight the crucial importance of cloud-resolving capability and the size of fine mesh for heavy-rainfall QPFs in Taiwan.

1 Introduction

The quantitative precipitation forecasting (QPF) is one of the most challenging areas in modern numerical weather prediction (e.g., Golding, 2000; Fritsch and Carbone, 2004; Cuo et al., 2011), especially for extreme events that have high potential for hazards. With its steep and complex topography, Taiwan over the western North Pacific (Fig. 1) experiences extreme rainfall rather frequently mainly during two periods: the typhoon (July-October) and mei-yu (May-June) seasons (e.g., Kuo and Chen, 1990; Wu and Kuo, 1999; Jou et al., 2011; Chang et al., 2013), when landslides and flash floods in/near the mountains and flooding over low-lying plains and urban areas are the main hazards (e.g., Wang et al., 2012b, 2013b, 2016b). In order to better prepare for these hazards and reduce their impacts, model QPFs and their verifications, especially over heavy-rainfall thresholds from large events, are thus very important for Taiwan. Of course, to identify where the model can make significant improvements in QPFs and what approaches are effective to achieve them are also crucial (e.g., Clark et al., 2011).

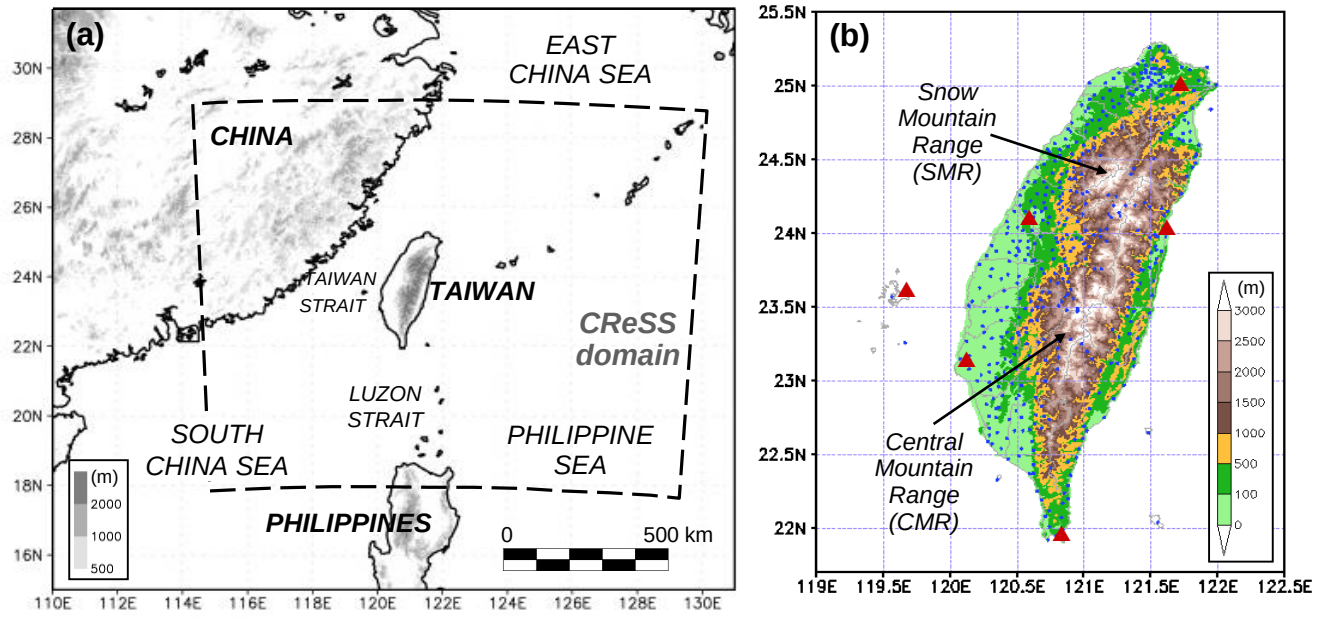

Figure 1: (a) The geography and topography (m, shading) surrounding Taiwan and the domain of 2.5-km CReSS (thick dashed box), and (b) the detailed terrain of Taiwan (m, color) and the locations of rain gauges (blue dots) and land-based radars (scarlet triangles) used to produce the reflectivity composites by the Central Weather Bureau (CWB). The two major mountain ranges in Taiwan, the Central Mountain Range (CMR) and Snow Mountain Range (SMR), are marked in (b).

For the mei-yu season in Taiwan, earlier studies mainly employed the widely-used, standard categorical measures (see Section 2.4) to evaluate the performance of models such as the Mesoscale Model version 5 (MM5) at thresholds up to 50 mm per 12 h (e.g., Chien et al., 2002, 2006; Yang et al., 2004). Their results show that the models at the time had some skill in predicting rainfall occurrence at thresholds ≤ 2.5 mm, but little skill at 50 mm and above. In recent years, several studies (e.g., Hsu et al., 2014; Li and Hong, 2014; Su et al., 2016; Huang et al., 2016) have also examined the QPFs by the Weather Research and Forecasting (WRF) model (Skamarock et al., 2005) running at the Central Weather Bureau (CWB) at 5-km grid spacing (Δx), including its ensembles. These studies indicate improvements over earlier models at thresholds up to 50-100 mm (per 12 h) over the previous decade. However, the skill at 150-200 mm and

beyond is still limited, even with probability-matching (e.g., Ebert, 2001) within the forecast range of 24 h (see e.g., Figs. 9 and 10 of Huang et al., 2016).

Figure 2 shows the threat scores (TSs, defined as the fraction of hits among all verification points that are either observed or predicted, or both, at the specified rainfall threshold; $0 \le TS \le 1$, further details in Section 2.4) of day-1 (0-24 h) and day-2 (24-48 h) QPFs for May and June of 2013 and 2014 by the CWB WRF model and several products from their 20-member WRF ensemble prediction system (WEPS, e.g., Hong et al., 2015), all with Δx = 5 km, as an example. These plots are produced for each month at the CWB for routine verification (within a range of 48 h) since 2013, and are similar to those in Huang et al. (2015, 2016). In addition to deterministic forecasts, the scores also include those using probability-matching techniques (PM and NPM, e.g., Ebert, 2001; Fang and Kuo, 2013), which may provide some benefit over the ensemble mean (WEPS) over thresholds of about 50-200 mm (e.g., Su et al., 2016; Huang et al., 2016). In Fig. 2, one can see that the TSs are no higher than 0.07 at 100 mm (per 24 h) and 0.03 at 200 mm (and TS = 0 at and above 300 mm) for either day 1 or day 2 in the two mei-yu seasons, in line with the review above. The scores in June also tend to be lower compared to May, likely due to more events of thermally-driven, localized rainfall with low predictability (e.g., Chen and Chen, 2003; Chen et al., 1999; Paul et al., 2018). Nevertheless, effective strategies and methods to improve the skill level at thresholds near 100-150 mm and beyond are needed.

Wang (2015, hereafter referred to as W15) evaluated the QPFs, within 3 days, by a cloud-resolving model (CRM), the Cloud-Resolving Storm Simulator (CReSS; Tsuboki and Sakakibara, 2002, 2007), for all 15 typhoons that hit Taiwan in 2010-2012. With Δx = 2.5 km, a grid size more comparable to research (e.g., Wang et al., 2005, 2011; 2013a, also Bryan et al., 2003; Done et al., 2004; Clark et al., 2007; Roberts and Lean, 2007), these deterministic forecasts show superior performance in QPFs, with TSs of 0.38, 0.32, and 0.16 at thresholds of 100, 250, and 500 mm, respectively, for all typhoons on day 1 (0-24 h, cf. his Fig. 13). Even on day 3 (48-72 h), the corresponding TSs are 0.21, 0.12, and 0.01. Thus, the skill by this CRM over the thresholds of 100-500 mm is remarkably high for typhoon rainfall in Taiwan.

Moreover, as summarized in Wang (2016), W15 found a strong positive dependency of categorical scores on overall rainfall amount (which represents event magnitude). That is, the larger the rain, the higher the scores, and the better the model performs. For example, the TSs at the same thresholds (100, 250, and 500 mm) for his top-5 events (roughly top 5%) on day 1 are 0.68, 0.49, and 0.24, respectively (Fig. 1 of Wang, 2016), all at least 1.5 times higher than their counterparts for all typhoons. An important implication of this finding is that the model QPFs for extreme events *may not* be accurately assessed through categorical statistics without proper classification to isolate them from ordinary events, and particularly not by taking arithmetic mean of TSs of multiple forecasts. The study of W15 also predicts the dependency, as a fundamental property, to exist in other rainfall regimes. Therefore, the main purpose of this study is three-fold: 1) to assess the skill of the 2.5-km CReSS in predicting mei-yu rainfall at a higher resolution than before, especially for heavy to extreme rainfall events, 2) to clarify whether the dependency property in categorical scores also exists in the mei-yu regime in Taiwan? and 3) if the QPFs by CReSS prove to be improved, why or where its strength lies? As none of these above questions has been addressed before, to answer them are our objectives.

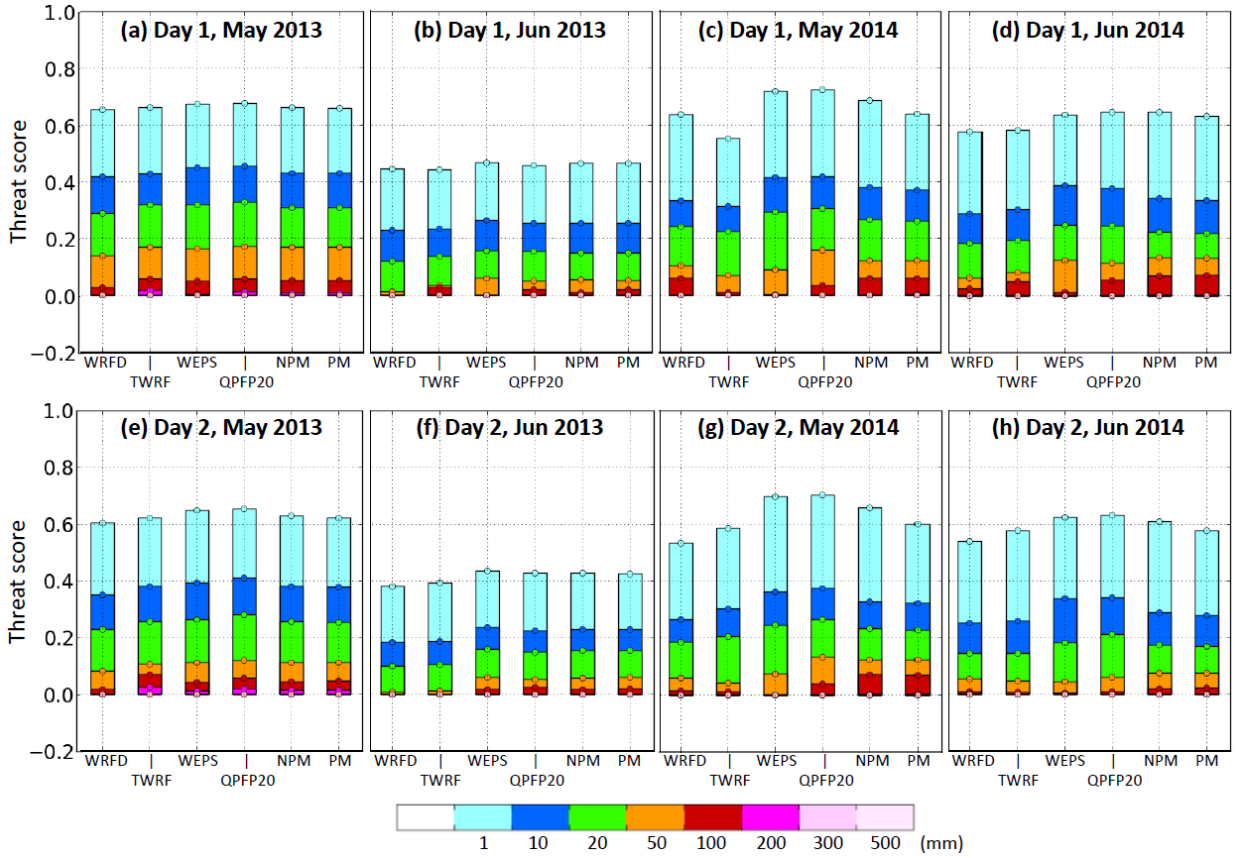

Figure 2: The TS of 0-24-h QPFs (day 1) for (a) May and (b) Jun of 2013, and (c) May and (d) Jun of 2014, respectively, at selected thresholds over 1-500 mm (per 24 h, scale at bottom) by two deterministic forecasts from WRF (WRFD) and the Typhoon WRF (TWRF) and four ensemble forecasts from the 20-member WRF Ensemble Prediction System: ensemble mean (WEPS), top 20% (QPFP20), and WEPS employing the probability matching (PM) and new PM (NPM) techniques. (e)-(h) As in (a)-(d), but showing the TS of 24-48-h QPFs (day 2), respectively.

In Section 2, the model, data, and methodology are described. In Section 3, the overall scores of QPFs for groups with different event magnitudes are presented and compared with previous results. Then in Section 4, examples are selected to illustrate how the CRM performs in real-time forecasts and where its strength lies. Aspects related to the dependency property are further discussed in Section 5, and our conclusions are given in Section 6.

2 Data and Methodology

2.1 The CReSS model and its forecasts

The CReSS model is a non-hydrostatic, compressible CRM with a single domain without nesting (Tsuboki and Sakakibara, 2002, 2007), and it has been used for weather forecasts in Taiwan since 2006 (http://cressfcst.es.ntnu.edu.tw/, W15; Wang et al., 2013, 2016a). Starting from July 2010, a grid size of 2.5 km is utilized, with a domain of 1500 × 1200 km^2 since May 2012 (Fig. 1a and Table 1). In CReSS, cloud formation, development, and all related processes are explicitly treated using a bulk cold-rain microphysical scheme with six species (Lin et al., 1983; Cotton et al., 1986; Murakami, 1990; Ikawa and Saito, 1991; Murakami et al., 1994): vapor, cloud water, cloud ice, rain, snow, and graupel without any cumulus parameterization scheme (Table 1). Other sub-

grid scale processes parameterized in the model include turbulent mixing in the planetary boundary layer with a 1.5-order closure (Deardorff, 1980; Tsuboki and Sakakibara, 2007), as well as surface radiation and momentum/energy fluxes (Kondo, 1976; Louis et al., 1982; Segami et al., 1989). These physical options are identical to W15, and also given in Table 1.

Season	2012	2013 and 2014
Projection	Lambert Conformal (center at 120°E, secant at 10°N and 40°N)	
Grid spacing (km)	2.5 × 2.5 × 0.2-0.663 (0.5)*	
Grid dimension (*x*, *y*, *z*)	600 × 480 × 40	
Domain size (km)	1500 × 1200 × 20	
Forecast frequency	Every 6 h (at 0000, 0600, 1200, and 1800 UTC)	
Forecast range	72 h	78 h
IC/BCs (including sea surface temperature)	NCEP GFS analyses/forecasts (at 26 levels)	
	1° × 1°	0.5° × 0.5°
Topography	Real at (1/120)° spatial resolution (~0.9 km)	
Cloud microphysics	Bulk cold-rain scheme (Lin et al., 1983; Cotton et al., 1986; Murakami, 1990; Ikawa and Saito, 1991; Murakami et al., 1994)	
PBL/turbulence	1.5-order closure with prediction of turbulent kinetic energy (Deardorff, 1980; Tsuboki and Sakakibara, 2007)	
Surface processes	Energy/momentum fluxes, shortwave and longwave radiation (Kondo, 1976; Louis et al., 1982; Segami et al., 1989)	
Substrate model	41 levels, every 5 cm to 2 m	

Table 1: The basic configuration, initial/boundary conditions (IC/BCs), and physical packages of the 2.5-km CReSS used for real-time operation in 2012-2014. * The vertical grid spacing of CReSS is stretched (smallest at bottom), and the averaged spacing is given in the parentheses.

The operational analyses and forecasts by the Global Forecasting System (GFS, Kanamitsu, 1989; Kalnay et al., 1990; Moorthi et al., 2001; Kleist et al., 2009) of the National Centers for Environmental Prediction (NCEP), produced every 6 h (at 26 levels), were used as initial and boundary conditions (IC/BCs) for CReSS (Table 1). The CReSS model is also run four times a day, each out to 72 h (now 78 h). At the lower boundary, terrain data at 30" resolution (roughly 900 m) and the NCEP analyzed sea surface temperature are also provided. With its limited domain size, the atmospheric evolution in CReSS is forced by the NCEP forecasts, especially at longer ranges. Note that since 2013, the IC/BCs from the GFS have increased the resolution from 1° × 1° to 0.5° × 0.5°, but all other settings are kept the same during our study period (Table 1).

2.2 Data

The observational data used include synoptic weather maps from the CWB, the vertical maximum indicator reflectivity composites every 30 min from land-based radars, and hourly rainfall data from about 440 gauges in Taiwan for QPF verification (Fig. 1b). Along with NCEP gridded final analyses (on 1° × 1° grid), the weather maps are used to identify

and synthesize the occurrence of favorable factors to heavy rainfall among events with different magnitude (to be described in Section 2.3). For selected heavy-rainfall cases, the radar composites are compared with the CReSS forecasts to assess the quality of the QPFs in Section 4.

Group	Criterion (of 10% gauges)	No. of segments (%)	No. of all points (N)	No. of points ($H + M + FA$) at threshold (mm)			
				50	100	250	500
A+	≥ 130 mm (a subset of A)	13 (3.9)	5622	3807	2453	490	32
A	≥ 50 mm	61 (18.1)	26826	11000	4889	675	47
B	≥ 25 mm, but not A	75 (22.3)	33018	4279	1078	98	4
C	≥ 10 mm, but not B	88 (26.1)	38583	1675	281	10	3
D	≥ 1 mm, but not C	67 (19.9)	29267	266	32	0	0
X	< 1 mm	46 (13.6)	20067	59	20	4	0
All	A through D plus X	337 (100.0)	147761	17279	6300	787	54

Table 2: The classification criteria using (at least) 10% of rain gauges with highest 24-h accumulated rainfall (0000-2400 or 1200-1200 UTC) over Taiwan, and the results in the number of 24-h segments (and percentage) and total points (sites) of $H + M + FA$ at selected rainfall thresholds (mm) for the different groups. During the mei-yu seasons of 2012-2014, the total N is 148776 and on average there are 442 rain gauges per segment. The points of $H + M + FA$ are based on the statistics of day-1 (0-24 h) QPFs, and N is also given (with no threshold).

2.3 Verification period classification

In this study, objective categorical statistics (e.g., Schaefer, 1990; Wilks, 2011) are used to verify QPFs mainly because: 1) the ability of models to predict the heavy rainfall at the correct location is imperative in Taiwan, since its primary hazards are landslides and floods, and 2) our results can be easily compared with earlier studies. Here, 24-h QPFs are chosen because: 1) the bulk rainfall accumulation from mei-yu events, as for typhoons, is our main concern rather than the rain over shorter periods, especially at longer ranges (days 2-3), and 2) the issue of double penalty on high-resolution QPFs (e.g., Ebert and McBride, 2000) is less serious using a longer accumulation period. Although the CReSS forecasts are made four times a day, only those from 0000 and 1200 UTC are evaluated in this study.

A total of 366 target segments (0000-2400 and 1200-1200 UTC) in May-June, 2012-2014 are classified into several groups based on the observed rainfall using the following criteria, as summarized in Table 2. Groups A, B, C, and D are those periods with at least 10% rain gauges reaching 50, 25-50, 10-25, and 1-10 mm, respectively, while group X is the remaining periods with little or no rain. The full classification results (Table 3) give a total of 337 segments, excluding those under typhoon influence. Groups A-D individually account for about 18-26% and are comparable in sample size, while the driest group X is about 14% (Tables 2 and 3). These five groups are exclusive to each other, and the results without classification will be referred to as the "all" group. From group A, a subset of A+ that has ≥ 10% sites reaching 130 mm is identified and represents the most-rainy 4% in our sample with the highest hazard potential. The spatial distribution of mean mei-yu rainfall per season in 2012-2014, with a peak amount of about 1700 mm, is shown in Fig. 3 and resembles the climatology (e.g., Yeh and Chen, 1998; Chien and Jou, 2004; Chi, 2006; Wang et al., 2017).

Year	Month	Time (UTC)	Date in month			Segments included (A-D, X)
			1-10	11-20	21-31 (or 21-30)	
2012	May	0000	XAABDXXXBB	CCXXCBAAAB	XXDXDCAAABC	31
		1200	CAADXXXBCC	CXXCBBAB**A**D	XXXXDBAABBD	31
	Jun	0000	CCBCCCCB**AA**	**AA**AAABBTTT	TCCDDCTTTD	23
		1200	DBCDCDBA**AA**	**A**AAABBTTTT	TCDDDTTTTD	21
2013	May	0000	CCCCBBCCDA	AACCCABAA**A**	CBCCCDDDDDX	31
		1200	CCDCACCDD**A**	BBCCCABABA	BBCCDDDDDXX	31
	Jun	0000	XXCBCCXXCB	BBABCDDDXX	BDBCCXXXXD	30
		1200	XDBCCDXDCB	BABBDDDXXB	CBBCXXXXXD	30
2014	May	0000	CCBBBBCCCD	DCBD**A**BXBA**A**	ADDCDCCBBBC	31
		1200	CBDABCDCDD	CBDAAXBAA**A**	BDCCDBBABCD	31
	Jun	0000	XDACAABBBC	CTTTTTTDDB	DCBCCDXCAC	24
		1200	XACBAABBDC	TTTTTTTDBD	CCBCDXDBAC	23
Total			A+: 13, A: 61, B: 75, C: 88, D: 67, X: 46 (T: 29)			337

Table 3: The full classification result for all the 24-h verification periods during the three mei-yu seasons of 2012-2014. For each month, the first (second) row gives the results of 0000-2400 (1200-1200) UTC. While the groups of A-D and X are denoted by their corresponding letter, a bold A indicates group A+ (a subset of A) and T marks the periods influenced by tropical cyclones and thus excluded from study.

2.4 Categorical measures of model QPFs

As mentioned, the 24-h QPFs by CReSS are verified against the rain gauge data, at three different ranges of 0-24, 24-48, and 48-72 h (days 1-3). For this purpose, objective skill scores computed from the standard 2×2 contingency table (or the categorical matrix) at a wide range of 14 thresholds from 0.05 to 750 mm are adopted. These measures include the TS (also called critical success index), bias score (BS), probability of detection (POD), and false alarm ratio (FAR), respectively defined as (e.g., Schaefer, 1990; Wilks, 2011; Ebert et al., 2003; Barnes et al., 2009)

$$\mathrm{TS} = H/(H + M + FA), \quad (1)$$

$$\mathrm{BS} = (H + FA)/(H + M) = F/O, \quad (2)$$

$$\mathrm{POD} = H/(H + M) = H/O, \text{ and} \quad (3)$$

$$\mathrm{FAR} = FA/(H + FA) = FA/F, \quad (4)$$

where H, M, and FA are the counts of hits (both observed and predicted), misses (observed but not predicted), and false alarms (predicted but not observed), respectively, among a total number of N verification points. Here, $N = H + M + FA + CN$, where CN is the correct negatives (neither observed nor predicted), and the total counts in observation (O) and forecast (F) are simply $O = H + M$ and $F = H + FA$. The values of TS, POD, and FAR are all bounded by 0 and 1, and the higher (lower) the better for TS and POD (FAR). For BS, its value can vary from 0 to ∞ (or $N - 1$ in

practice), but unity is the most ideal and implies no bias. Also, BS >(<) 1 implies overestimation (underestimation) of the events. By interpolating the model QPFs onto the gauge sites that serve as verification points (i.e., $N \approx 440$ per segment) using the bi-linear method, the counts of *H*, *M*, *FA*, and *CN* at any given threshold can be easily obtained for each segment. Although the density of rain gauges varies to some extent (roughly every 5-10 km in the plains and ≥10-20 km in the mountains, cf. Fig. 1b), their weights are assumed equal (e.g., Wang, 2014). For any group (e.g., A+) at a given threshold, the scores are obtained from a single 2 × 2 table that combines the entries from all segments, so that the sample sizes are maximized (cf. Table 2, e.g., W15). This practice also remedies the issue of sampling inhomogeneity and increases the stability of results, especially toward the high thresholds, as long as the points involved in the matrix are not too few in number (cf. Table 2). Since neither the observation nor the forecast ever reached 750 mm (per 24 h) during the study period, results for 13 thresholds from 0.05 up to 500 mm (the next highest threshold) are presented in later sections. Also, only 24-h QPFs are evaluated in the current study. Except for the categorical matrix, subjective visual verification is also used in the selected examples (Section 4).

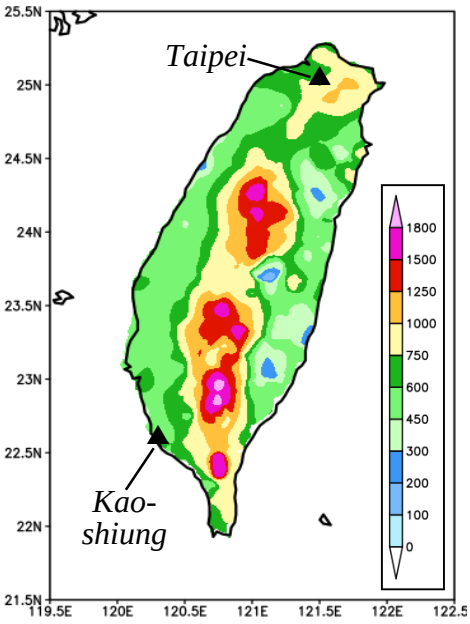

Figure 3: Spatial distribution of mean total rainfall (mm) per mei-yu season (1 May through 30 Jun) in 2012-2014. The cities of Taipei and Kaoshiung are marked.

3 Mei-yu QPFs in 2012-2014

3.1 Overall skill by the 2.5-km CReSS

Following the method described above, the categorical matrices across the thresholds are obtained and the overall skill of CReSS in mei-yu QPFs during 2012-2014 is shown in Fig. 4 using the performance diagram. Proposed by Roebber (2009), the diagram uses the success ratio (SR = 1 – FAR = *H*/*F*) and POD as its two axes, and can also depict the TS (gray curved isopleths, higher toward upper-right) and BS (brown dotted lines) simultaneously. In Fig. 4, the scores from forecasts at both 0000 and 1200 UTC for segments (of 24 h) in groups A+, A to D, and all periods (A-D plus X, cf. Table 2) at 13 thresholds are shown for ranges of day 1, 2, and 3, respectively. The "all" group (black) shows the

overall skill for all mei-yu rainfall without classification, and its TS for day-1 QPFs decreases slowly from 0.6 at 0.05 mm to 0.18 at 100 mm, 0.15 at 250 mm, and 0.09 at 500 mm (Fig. 4a). Over heavy-rainfall thresholds ≥ 160 mm, the TSs of 0.09-0.16 are significantly higher than those reviewed in section 1. Even on day 2, the TSs remain at 0.11 to 0.06 over 160-500 mm, and above 0.03 up to 350 mm on day 3 (Figs. 4c,e).

When all segments are stratified by the observed event magnitude, the TSs are higher and the skill better for larger events than smaller ones, following the order of A+ then A to D for all thresholds at all three ranges without any exception (Fig. 4), while each individual curve mostly decreases with threshold when rain areas reduce in size (as shown in Fig. 5). Thus, the positive dependency of categorical measures on rainfall amount is also strong and evident in mei-yu QPFs in Taiwan, as predicted by W15, and the second question in our objectives is answered. Linked to this dependency, the TSs for large events are also higher than those for the "all" group from the entire sample. For the most hazardous group A+, for example, the TS on day 1 is 0.34 at 100 mm, 0.24 at 250 mm, and 0.16 at 500 mm (per 24 h, Fig. 4a). On days 2 and 3, the corresponding TSs are 0.32, 0.15, and 0.07 (Fig. 4c), and 0.25, 0.05, and 0.00 (Fig. 4e), respectively, all higher than their counterparts for the all group (except day 3 at 500 mm). Similar to some earlier studies (e.g., Chien et al., 2002, 2006; Chien and Jou, 2004; Yang et al., 2004), if we select TS ≥ 0.15 to indicate some predictive skill, then the QPFs by the 2.5-km CReSS have skill all the way up to 500 mm (per 24 h) on day 1, 250 mm on day 2, and 130 mm on day 3. Also, for A+, A, and all groups, the TSs of day-2 QPFs stay quite close to the values on day 1, and some are even identical, from low thresholds up to 200-250 mm. For day-3 QPFs compared to day 2, the same is true up to about 130 mm (Fig. 4, left column). Such results that some skill of heavy-rainfall QPFs still exists on days 2-3 are very encouraging. On the other hand, at thresholds ≥ 50 mm, the skill for B-D events (Fig. 4, right column) are limited (TS ≤ 0.08) when the rain areas are relatively small (with $O/N \leq 6\%$, Fig. 5), but as discussed in W15, this is not important due to low hazard potential.

Another fairly subtle but important feature in Fig. 4 is that the TSs of all, A, and A+ groups decrease only marginally at times, or do not drop at all, across some heavy-rainfall thresholds, particularly on days 1-2, despite the reduction in rain-area size (left column). Some examples include the TSs for group A+ over 100-350 mm on day 1 (drops from 0.34 to 0.21), and those for group A over the same thresholds on day 1 (from 0.23 to 0.15) and over 100-250 mm on day 2 (from 0.20 to 0.14). Even on day 3, the decrease of A and "all" curves from 160 to 350 mm is rather slow, although the TSs there are only 0.03-0.07 (Fig. 4e). Such a slow decline in TSs with thresholds indicates that in a relative sense, the model is more capable to produce hits toward the rainfall maxima, which occur more frequently in the mountains (cf. Figs. 1b and 3).

By definition, both POD and SR cannot be lower than the TS [cf. Eqs. (1), (3), and (4)], and the ratio of POD/SR equals to the BS (thus, POD < SR if BS < 1 and vice versa). In Fig. 4, the PODs start at 0.05 mm from nearly perfect values of 0.98-0.99 for days 1-3 for group A+, at least 0.9 for A, and ≥ 0.72 for all segments (left column). For these three groups, the PODs at 250 mm remain at least 0.32 on day 1, 0.21 on day 2, and 0.05 on day 3. Like the TS, the skill in POD for mei-yu rainfall indeed decreases quite significantly with forecast range (lead time), particularly toward high thresholds, mainly due to error growth and the reduction in predictability, but some skill still exists at 130 mm even on day 3, with POD = 0.16 and TS = 0.07 (for all segments). The SR values (and thus FAR) are again the best for group A+ and ≥ 0.36 across all thresholds on day 1, including 500 mm (Fig. 4a). On day 2, the SRs for A+ over

130-500 mm decrease but not by too much, and the values over 10-250 mm even increase on day 3 (Figs. 4c,e). Often, the SR for A+ is considerably higher than those for A and all events regardless of forecast range, particularly over heavy-rainfall thresholds. Overall, the model also produces higher POD and SR (i.e., lower FAR) for larger events compared to smaller ones at all thresholds and all three forecast ranges in Fig. 4, with only a few exceptions after close inspection. This indicates that the high-resolution CReSS not only produces larger rainfall for large rainfall events, which leads to a higher TSs, but also produces larger rainfall for small events, which leads to lower SR values. In summary, as for typhoon rainfall (W15), the 2.5-km CReSS is the most skillful in predicting the largest events in the mei-yu season in Taiwan..

Next, the BS values are examined for over/under-prediction (i.e., above/below the diagonal line) in Fig. 4, where the threshold with O/N falling below 1% is marked to indicate values that might be potentially unstable and less meaningful. For day-1 QPFs, the BSs for all segments suggest slight under-prediction for low thresholds ≤ 10 mm (per 24 h), but some over-prediction (BS ≈ 1.25-1.5) across 50-350 mm (Fig. 4a). On the contrary, the model shows slight over-prediction over 0.05-75 mm for the largest events of group A+ (with BSs up to 1.15), but under-prediction toward higher thresholds, with the lowest BS of 0.52 at 350 mm. Mostly between the two curves mentioned above, the curve for group A stays closer to unity and is more ideal across nearly all thresholds (Fig. 4a). For B-D groups (Fig. 4b), their characteristics are similar to the All group, with BSs of 0.8-1.0 at low thresholds but generally some over-prediction across higher thresholds. However, their BS values rarely exceed 2.5, unless the O/N values drop to below 1%. The situation for BSs between different groups remains similar on days 2 and 3 (Figs. 4c-f), and the over-forecasting across the middle thresholds in group A (at all ranges) can be confirmed to come mainly from groups B-D, as groups A+ and A exhibit little or a much less tendency for over-prediction there (Fig. 4).

Toward the longer ranges of days 2 and 3, the BS values in general become smaller, particularly for the larger groups (Fig. 4, left column). Thus, the over-prediction in group A is reduced and the under-prediction in A+, which is the most important group, becomes more evident, especially toward the high thresholds (Figs. 4c,e). For example, the BS of day-2 QPFs for A+ is ideal and ≥ 0.8 up to 200 mm but declines to about 0.35 at 500 mm, but it is already below 0.4 at 130 mm on day 3. This indicates that for larger events, the error growth with lead time in the model tends to become less rainy, as reflected in the decrease in BS. Thus, the probability to under-forecast peak rainfall rises with lead time. For smaller events that do not produce much rainfall (i.e., B-D and X), a similar tendency does not exist or is weaker, and BS tends to be greater than unity. Thus, as exemplified here, the BSs from the larger and hazardous events can be quite different from those from all events, which are inevitably affected by the more frequent but small (unimportant) events. So, to say the least, one needs to practice caution in the interpretation of BS, which can also become unstable when O/N approaches zero (which inevitably happens at certain thresholds).

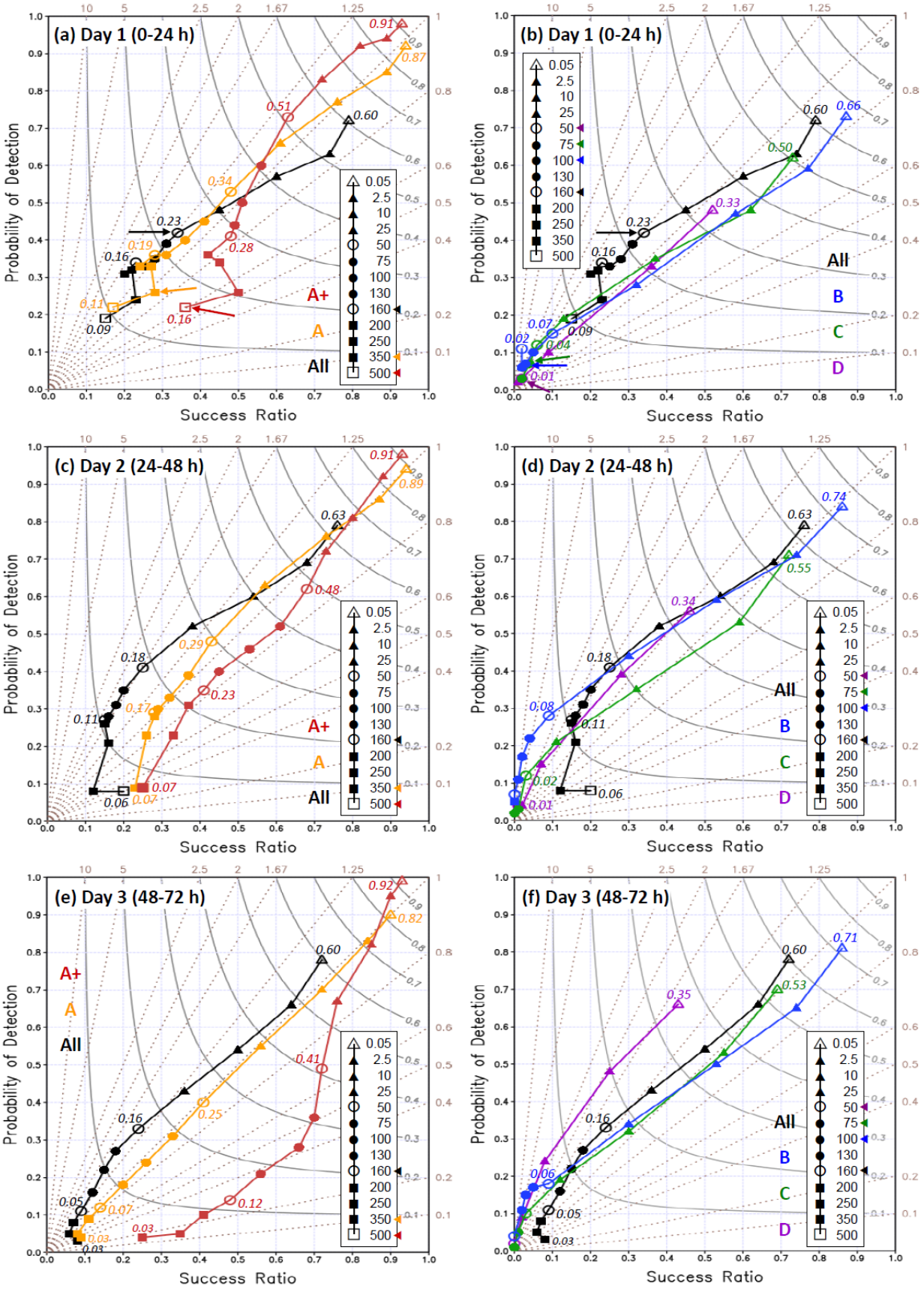
(a) Day 1 (0-24 h)
(b) Day 1 (0-24 h)
(c) Day 2 (24-48 h)
(d) Day 2 (24-48 h)
(e) Day 3 (48-72 h)
(f) Day 3 (48-72 h)
Probability of Detection
Success Ratio
A+
A
All
B
C
D
0.05
2.5
10
25
50
75
100
130
160
200
250
350
500

266

Figure 4: Performance diagrams of 24-h QPFs for (a),(b) day 1 (0-24 h), (c),(d) day 2 (24-48 h), and (e),(f) day 3 (48-72 h) by the 2.5-km CReSS, at 13 rainfall thresholds (inserts) from 0.05 to 500 mm, during three mei-yu seasons (May-Jun) in 2012-2014 in Taiwan. Results for groups A+, A, and All (All, B, C, and D) are plotted in left (right) column with different colors. TS values (rounded to two decimal places) are labelled at fixed thresholds of 0.05, 50, 160, and 500 mm (open symbols) or selected endpoints (smaller fonts), and data points with TS = 0 at high thresholds are omitted. For each group, the threshold where the observed rain-area size (*O*/*N*) falls below 1% is labeled in insert, and also marked by an arrow in (a),(b).

3.2 Improvement in heavy-rainfall QPFs

To assess the improvement in heavy-rainfall QPFs in mei-yu season, our results in Fig. 4 are compared to Fig. 2 and those reviewed in Section 1. However, the differences in model resolution should be noted. Overall, the "all" curves in Fig. 4 indicate that the 2.5-km CReSS exhibits better skill than those reviewed in Section 1 (with Δx as fine as 5 km at most), especially at thresholds above 100 mm (e.g., TS = 0.15 at 250 mm and 0.09 at 500 mm for day 1). With even higher TSs for larger and more hazardous events (groups A and A+), the improvement of heavy-rainfall QPFs in the present study from earlier results is therefore significant and quite dramatic. Thus, the first objective of this study is fulfilled, and the physical explanation will be further elaborated and discussed later in Section 4.

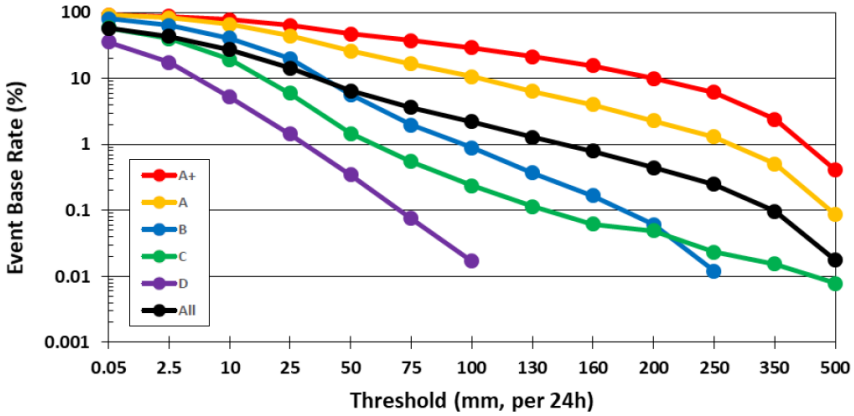

Figure 5: Observed rain-area size or base rate (*O*/*N*, %) of 24-h rainfall (same for days 1-3) in logarithmic scale used to compute the scores in Fig. 4

4 Examples of Model QPFs

Given the success of the CRM in its overall performance shown above, some examples of CReSS forecasts are selected and presented in this section for further examination and discussion. The main goal here is two-fold: 1) To illustrate how the model behaves and captures the rainfall with the corresponding scores in individual forecasts in detail, and thus 2) to identify where such a CRM has high skill in QPF and where it has limitations in Taiwan, thereby to shed light on the source of skill seen in Fig. 4. Since our focus is on heavy rainfall, the event during 9-12 June 2012, the largest during our study period, is chosen for illustration.

The event of 9-12 June 2012 spanned four days and contributes more than half the segments in group A+ (7 in 13, cf. Table 3), and the model's performance in predicting this event is thus highly relevant. In Fig. 6a, the observed 24-h rainfall distributions over Taiwan are shown every 12 h, from 1200-1200 UTC 8 June to 0000-2400 UTC 12 June 2012. Except for the first forecast period, all seven segments are qualified as A+ and five have a 24-h peak rainfall over 500 mm (those since 1200 UTC 9 June). Reminiscent to the season average (cf. Fig. 3), three rainfall maxima

from this lengthy event exist: over southern CMR, near the intersection of CMR and SMR in central Taiwan, and over northern Taiwan (Fig. 6a). The rain at the two mountain centers (cf. Fig. 1b) is much more persistent than that in northern Taiwan, which concentrated mainly over a 10-h period beginning 1400 UTC 11 June (Wang et al., 2016b). The southwestern plains also received considerable rainfall, especially around 9 June (Fig. 6a).

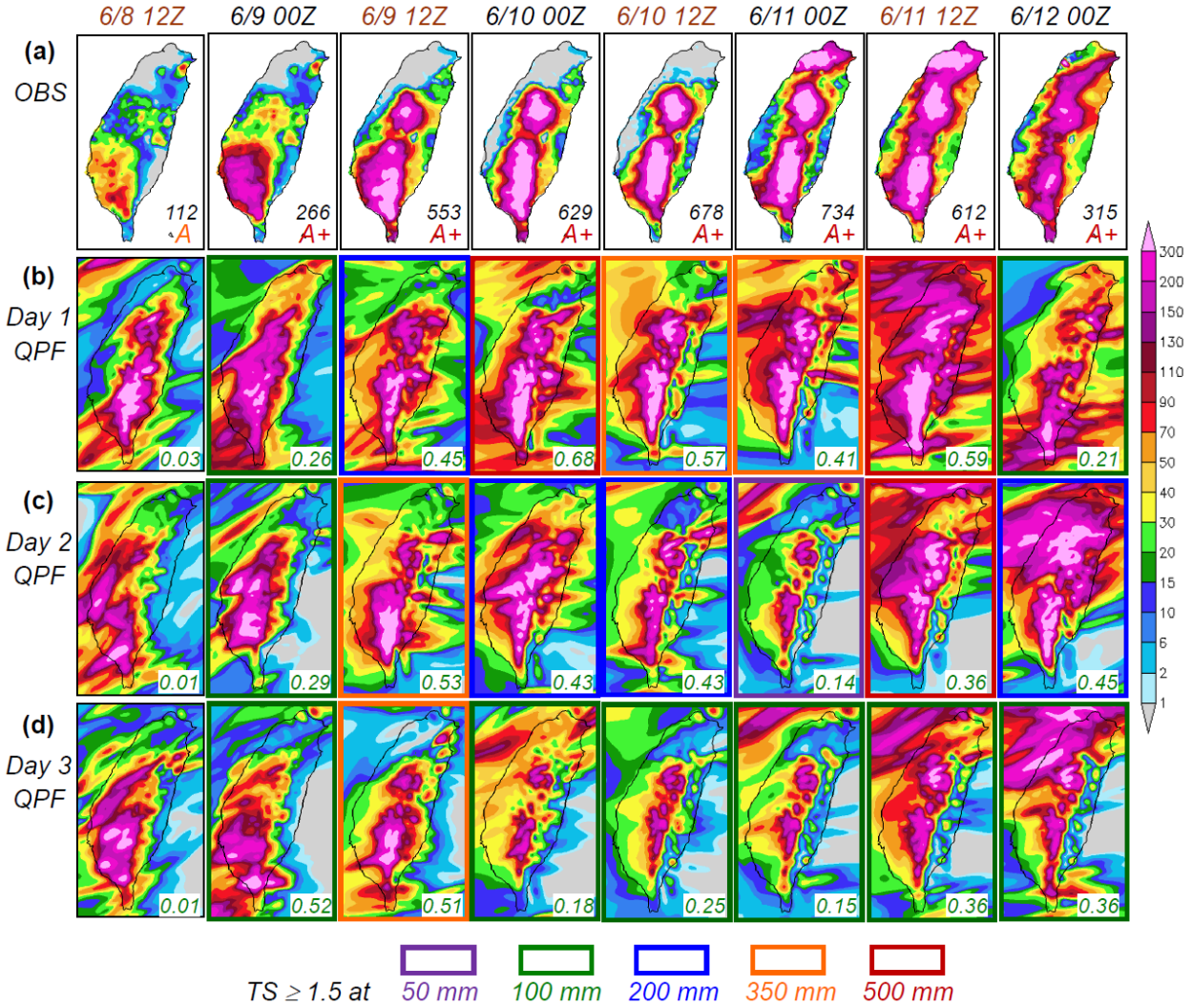

Figure 6: (a) The observed 24-h accumulated rainfall (mm, scale on the right) over Taiwan from 1200 UTC 8 Jun to 0000 UTC 13 Jun 2012, given every 12 h (from left to right), with the beginning time of accumulation (UTC) labeled on top (black for 0000-2400 UTC and brown for 1200-1200 UTC). (b) Day-1 (0-24 h), (c) day-2 (24-48 h), and (d) day-3 (48-72 h) QPFs valid for the same 24-h periods as shown in (a) by the 2.5-km CReSS (starting at 0000/1200 UTC under black/brown headings). In (a), peak 24-h rainfall (mm) and classification group are labeled. In (b)-(d), thick boxes in purple, green, blue, orange, and scarlet denote forecasts having a TS ≥ 0.15 at the threshold of 50, 100, 200, 350, and 500 mm (per 24 h), respectively, and the TS at 100 mm is also given (lower right corner).

The 24-h QPFs produced by the 2.5-km CReSS (at 0000 or 1200 UTC) in real time targeting the same periods as in Fig. 6a, at the ranges of days 1-3 are presented in Figs. 6b-d, with the general quality expressed by the TS at 100 mm (lower right corner inside panels) and thickened outline for TS ≥ 0.15 at the threshold of 50, 100, 200, 350, or 500 mm. The day-1 QPFs (Fig. 6b) are made from the forecasts starting (with initial time t_0) at the time of the heading,

while day-2 (Fig. 6c) and day-3 QPFs (Fig. 6d) in the same column (i.e., for the same target period) are those made 24 and 48 h earlier, respectively. In Fig. 6, this extreme and lengthy event was generally well captured by the model, especially on day 1 where the overall rainfall pattern and TS both tend to be better, as expected. The best day-1 QPF is for 0000-2400 UTC 10 June (TS = 0.68 at 100 mm and 0.40 at 500 mm), followed by the one for 1200 UTC 11-12 June (TS = 0.59 at 100 mm and 0.29 at 500 mm, columns 4 and 7, Fig. 6b). At longer ranges on days 2 and 3, the rainfall magnitudes produced over the mountains and southwestern plains are also comparable to observations, but the event starts somewhat too early and becomes less rainy during 10-11 June with apparent under-forecast (Figs. 6c,d). As a result, the TSs for the segments starting at 1200 UTC 8 June and during 10-11 June (columns 1 and 4-7) mostly increase from longer to shorter ranges, i.e., with better QPFs at later times. This relationship with range, however, does not hold true for the other segments, among which the day-3 and day-2 QPFs for the period of 1200 UTC 9-10 June (TS ≥ 0.51-0.53 at 100 mm and 0.20-0.31 at 350 mm) and the day-2 QPF for 1200 UTC 11-12 June (TS = 0.40 at 500 mm) are particularly impressive (columns 3 and 7). Compare to the rain over the terrain, the maximum across Taipei in northern Taiwan during 11-12 June was largely over lower and flatter regions (cf. Figs. 1b and 2) and more challenging for the model to predict at the right location (Fig. 6), an aspect that will be further elaborated on later. Note, nevertheless, that since the mountain regions are the only places where rainfall amounts reach 300 mm in both the observation and the model (Fig. 6), any hits at and above this threshold must occur in the mountains in this event.

Figure 7 shows the TS and BS of day-1 to day-3 QPFs from the runs made at a series of initial times, including 1200 UTC of 7-9 June and the next four from 0000 UTC 10 to 1200 UTC 11 June (top to bottom), and our focus is mainly over the thresholds ≥ 100 mm. Inside the panels, the observed event base rate (O/N, i.e., rain-area size, identical at the same threshold for the same target period) and the hit probability (H/N, note that $H/N \le O/N$) are given at selected points. With such information, it is easy to work out forecast base rate (F/N), POD, and SR, and thus how the model actually performed, particularly over the high thresholds. Some of the TSs at high thresholds mentioned above in relation to Fig. 6 can also be verified here.

Figures 7a-7f provide some examples on how the model did in predicting the commencement of the event (cf. Fig. 6, columns 1-3). As mentioned, the day-3 QPF made from 1200 UTC 7 June (Figs. 7a,b, blue curves) and day-2 QPF made one day later (Figs. 7c,d, red curves), both targeting 1200 UTC 9-10 June, are of fairly high quality. With rain areas (O/N) occupying 31%, 14%, and just 2% of Taiwan at 100, 200, and 350 mm, the day-2 QPF in Fig. 7c, with BS ≈ 0.6-1.1 (Fig. 7d), yields TSs of 0.53-0.31 at these thresholds. The day-3 QPF with t_0 at 1200 UTC 7 June, with less predicted rain and BS ≈ 0.3-0.6 (cf. Fig. 6d, column 3), the TSs are 0.51-0.2 (Figs. 7a,b). With TS at least 0.2 at 350 mm (an amount predicted only in southern CMR), both QPFs (for 1200 UTC 9-10 June) are quite skillful. Valid for periods with varying magnitude (B, A, and A+), the forecasts in Figs. 7a,b are also good examples to illustrate the dependency property (Fig. 4 and W15), where the rainfall amount apparently exhibits a larger influence on skill scores than the forecast range. In Figs. 7e,f, the TS curves at the three ranges (all for A+ events) are closer. In Fig. 8, the actual forecast near Taiwan between 42 and 69 h, from the run made at 1200 UTC 7 June, is compared with radar observations every 6 h to examine general rainfall locations. While a wind-shift line existed off eastern Taiwan, the surface mei-yu front was well to the north with prefrontal low-level southwesterly flow impinging on the island during

this period (also Wang et al. 2016b). Active convection constantly developed over the mountains in central and southern Taiwan and moved from the upstream ocean into the southwestern plains, and this scenario was well captured by the 2.5-km CReSS (Fig. 8), yielding a high-quality QPF on day 3 despite some under-forecast at thresholds ≥ 75 mm (cf. Figs. 7a,b).

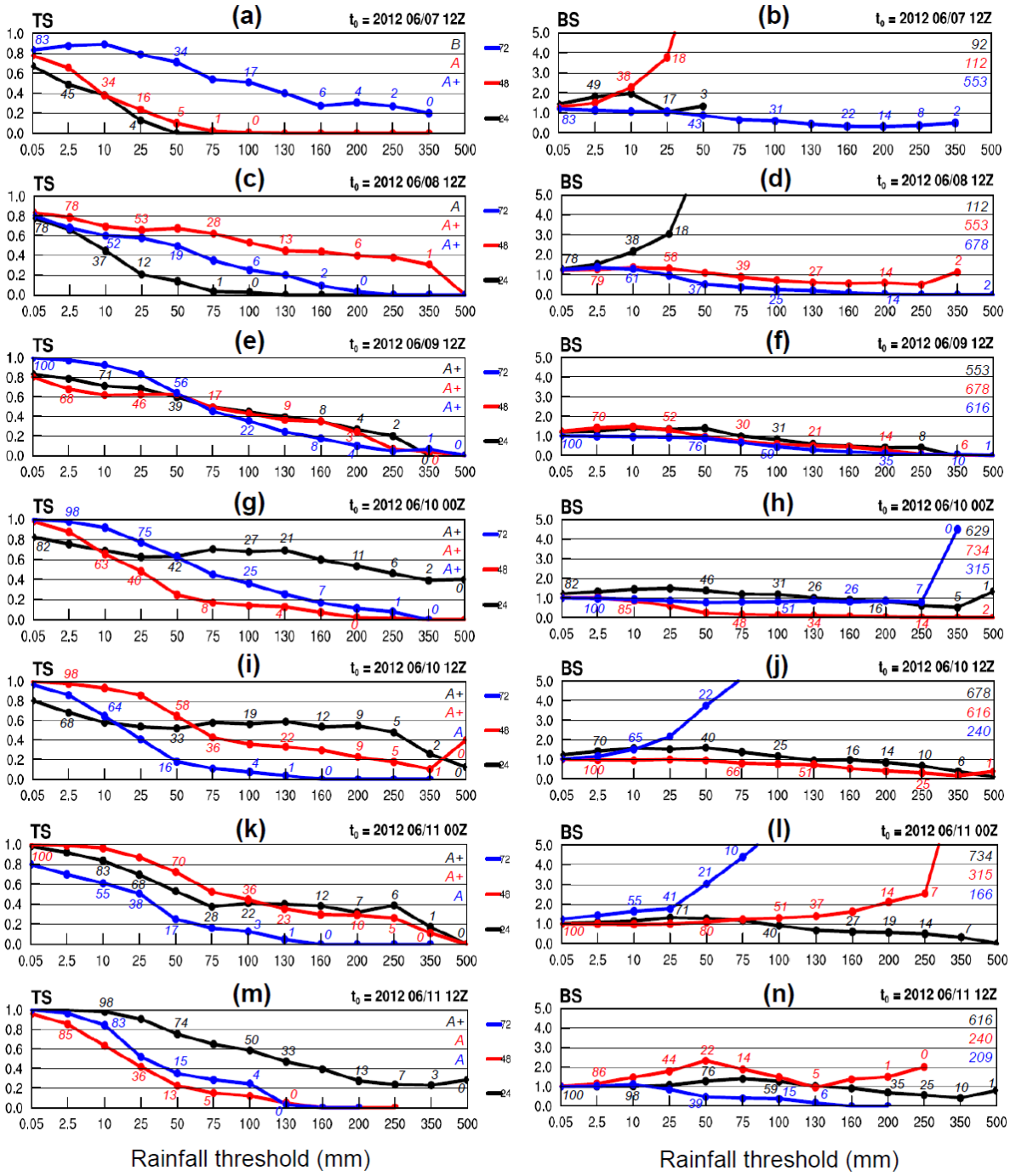

Figure 7: (a) TS and (b) BS of 24-h QPFs for day 1 (black), day 2 (red), and day 3 (blue) from the forecast made at 1200 UTC 7 Jun 2012 as a function of threshold (mm). (c),(d) to (m),(n) As in (a),(b), except for the forecasts made at 1200 UTC of (c),(d) 8 and (e),(f) 9 Jun, at (g),(h) 0000 UTC and (i),(j) 1200 UTC of 10 Jun, and (k),(l) 0000 UTC and (m),(n) 1200 UTC of 11 Jun, 2012, respectively. In left panels (for TS), the hit rate (*H*/*N*, %, rounded to integer) at selected points and the

classification group for each day are labeled. In right panels (for BS), the observed base rate (*O*/*N*, %) and peak 24-h rainfall (mm) are also given.

In the four following forecasts made on 10-11 June (Figs. 7g-n), while the dependency on event magnitude also exists, the QPFs made for A+ periods tend to have higher TSs above 75-100 mm at the shorter ranges (Figs. 7g,i,k), as mentioned. All of good forecast quality (cf. Figs. 6a,b, columns 4-7), the TSs of these day-1 QPFs can be as high as 0.48 at 250 mm and 0.40 at 500 mm. At 350-500 mm, such high TS occurs with *O*/*N* below < 10% (or even only 1%), and thus indicates remarkable model accuracy in predicting the peak rainfall at the correct location in the mountains in this event. Over thresholds ≥ 200 mm, BS values in Fig. 7 indicate that under-prediction for this extreme event occurs much more often than over-prediction, while they also tend to be closer to unity (with less under-forecast) for QPFs achieving higher TSs. Consistent with Fig. 4, an over-prediction is more likely to happen for smaller events (A or below), across low thresholds below 50 mm, and/or when the rain area becomes small. In Fig. 7, for example, BS ≥ 2 at high thresholds for A+ group occurs only when *O*/*N* approaches zero (Figs. 7h,n), with the lone exception in Fig. 7l on day 2. Overall, the model does not have a tendency to over-predict such a large event (cf. Fig. 6).

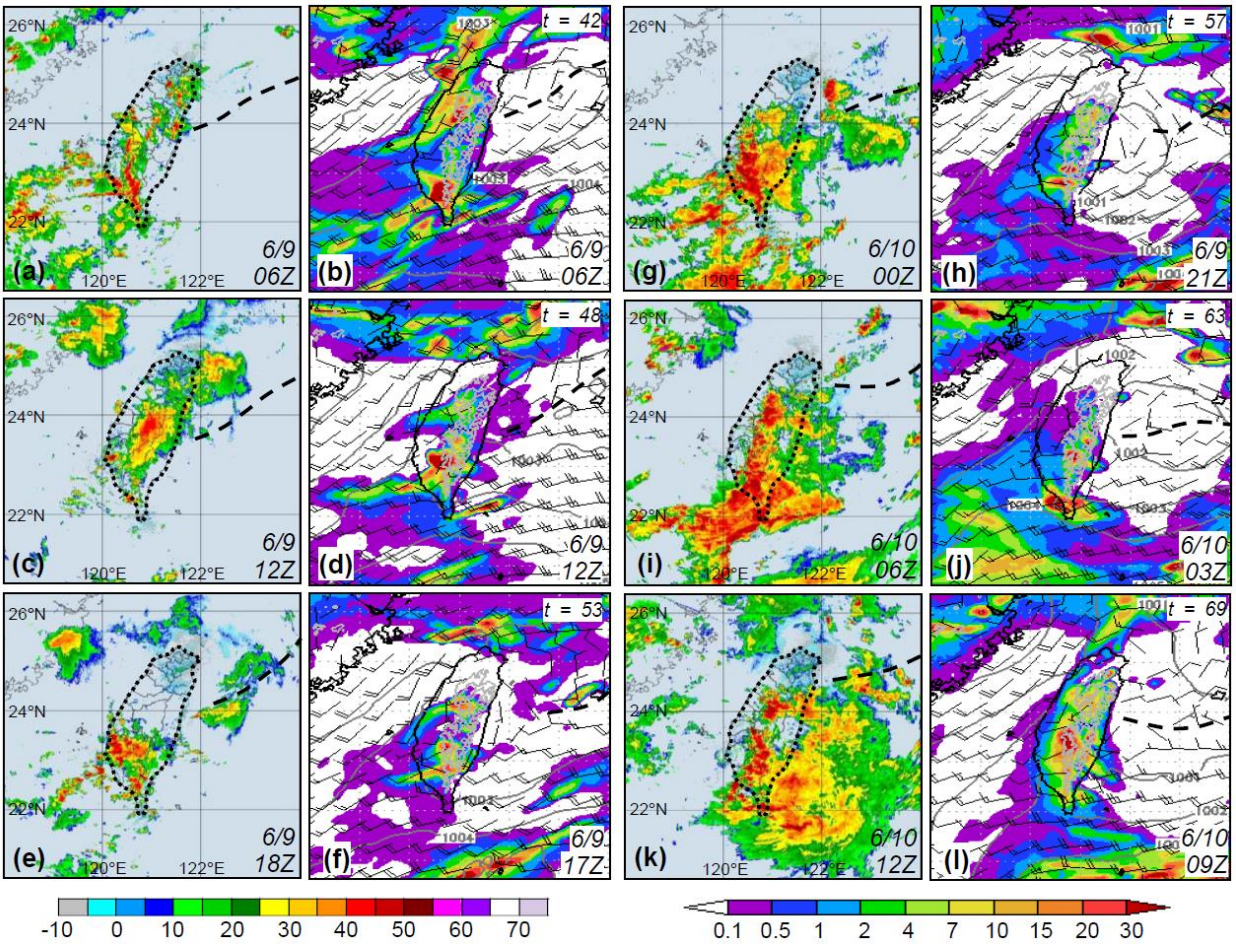

Figure 8: (First and third column) Radar reflectivity composite (dBZ, scale at bottom left) in the Taiwan area (width roughly 600 km) every 6 h from (a) 0600 UTC 9 Jun to (k) 1200 UTC 10 Jun, 2012 (original plots provided by the CWB). (Second and fourth column) The CReSS forecast, starting from 1200 UTC 7 Jun 2012, of sea-level pressure (hPa, every 1 hPa, over ocean only), surface wind (kts, barbs, at 10 m), terrain height at 1 and 2 km (gray contours), and hourly rainfall (mm, color, scale at bottom right) valid at the time or within 3 h of the radar composite as labeled [in UTC (forecast time

in h) at lower (upper) right corner] over the same area. The thick dashed lines mark the position of surface frontal or wind-shift line, based on NCEP gridded analyses for the observation (outline of Taiwan also highlighted).

The forecasts on days 1-2 produced by the run starting at 1200 UTC 10 June are compared with radar observations in Fig. 9. Together with Fig. 8, the radar panels cover the wettest 72 h (0600 UTC 9-12 June) of the entire event. During day 1 (Figs. 9a-h), the scenario remains similar to Fig. 8, and the model again was able to capture the mountain rainfall. The convection moving in from the Taiwan Strait, however, was too active and the rain along the western coast on day 1 was over-predicted with BSs ≈ 1.2-1.6 from 0.05 up to 100 mm (cf. Fig. 7j). Note that in Fig. 7, some over-prediction across low thresholds can also exist for group A+ and lowers the TS, which otherwise can often exceed 0.8 at and below 25 mm. In any case, the model's performance over the low thresholds is of secondary importance.

Since 1200 UTC 11 June, the mei-yu front gradually approached northern Taiwan, and its western section moved rapidly across the island after about 0000 UTC 12 June (Figs. 9i-p). Studied by Wang et al. (2016b), the heavy rainfall in northern Taiwan (during 1400-2400 UTC) was caused by quasi-linear convection that developed south of the front (Figs. 9i,k,m), along a convergence zone between the low-level flow blocked and deflected by Taiwan's topography, and unblocked flow further to the northwest (but still prefrontal) in the environment (also e.g., Li and Chen, 1998; Yeh and Chen, 2002; Chen et al., 2005; Wang et al., 2005). In the model forecast, with apparent errors in the position and moving speed of the front (Figs. 9i-p), it is highly challenging to produce a similar system at the correct location and time even when the overall scenario surrounding northern Taiwan are reasonably predicted. In the simulation of Wang et al. (2016b), the rainbands cannot be fully captured even with a finer grid of Δx = 1.5 km and the NCEP final analyses as IC/BCs. Likely mainly linked to the IC/BCs, the position error of the front in this case is still a major error source for the rainfall associated with the front. Thus, although the model did indicate a real possibility of heavy rainfall in northern Taiwan in Fig. 9, the high TS of 0.4 at 500 mm on day 2 (Fig. 7i) came from the mountains, where the rainfall prediction is clearly more accurate (cf. Figs. 6a,c, column 7), consistent with Walser and Schär (2004). Of course, the day-1 QPF with t_0 = 1200 UTC 11 June performed better in northern Taiwan than our example, but the goal here is to illustrate the relatively high accuracy to predict heavy rainfall phase-locked to the topography versus the low accuracy for rainfall produced by transient systems over low-lying plains.

The above example, together with other cases including those on 20 May 2013 and 20-21 May 2014, (cf. Table 3, not shown), suggests a lower accuracy and a more challenging task for model QPFs to capture the heavy rainfall produced by transient systems often in close association with the mei-yu front, compared to topographic rainfall in Taiwan. Even though the overall scenario is reasonably and realistically predicted (cf. Figs. 8 and 9), some position errors on the mei-yu front are almost inevitable and the intrinsic predictability can limit the accuracy of the QPF (e.g., Hochman et al., 2021). Also, for such rainfall caused by transient systems, categorical statistics are known to be less effective in verifying model QPFs (e.g., Davis et al., 2006; Wernli et al., 2008; Gilleland et al., 2010). However, for the quasi-stationary, phase-locked rainfall over the topography in the majority of large events (in both mei-yu and typhoon seasons, e.g., Chang et al., 1993; Cheung et al., 2008) in Taiwan, they are still valid and useful as shown herein. As model resolution increases, both the topography and deep convection can be better resolved, leading to improved QPFs over the terrain. Thus, through the ananlysis in this section, the third question in our objectives can be answered to a certain degree.

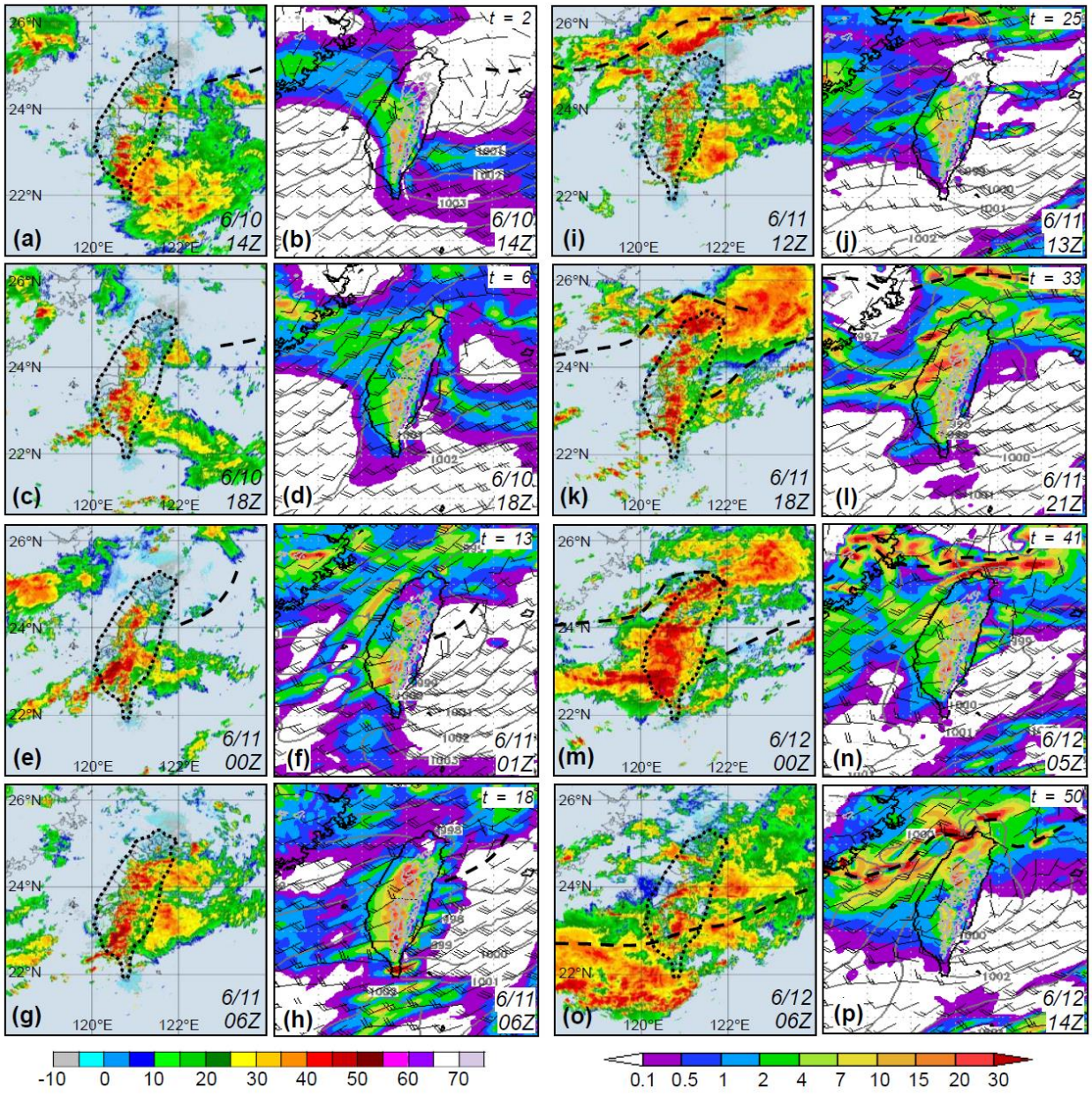

Figure 9: As in Fig. 8, but showing (columns 1 and 3) radar reflectivity composite (dBZ) at (a) 1400 UTC 10 Jun and every 6 h from (c) 1800 UTC 10 Jun to (o) 0600 UTC 12 Jun, 2012, and (columns 2 and 4) the CReSS forecast, starting from 1200 UTC 10 Jun 2012, of sea-level pressure (hPa), surface wind (kts), and hourly rainfall (mm) valid at the time or within up to 8 h (towards the end) of the radar composite (as labeled).

5 Dependency of Skill Scores to Event Size

In Section 3, a positive dependency in categorical measures by CReSS, including TS, POD, and FAR, on rainfall amount is shown for the mei-yu regime in Taiwan, as predicted. Also discussed in W15, this property arises mainly due to the positive correlation between the scores and rain-area sizes, as illustrated in Fig. 10 with a correlation coefficient $r = 0.89$ for the mei-yu regime. However, to explore whether the model is indeed more skillful in predicting

larger rainfall events, further analysis with the factor of rain-area size removed is needed. Different from W15, our approach here is described below.

For each segment, the statistics (*H*, *M*, *FA*, and *CN*) at 13 fixed thresholds of 0.05-500 mm, each occurring at a certain *O*/*N* (if the threshold ≤ the observed peak amount), are known. The observed base rate (0-100%) is divided into bins every 5% except at 0-5%, where it is subdivided into 0-0.5, 0.5-2, and 2-5% to give more comparable sample size. For each group (A+ or A-D), the statistics are then summed for each bin regardless of their rainfall threshold. Thus, those in the same bin come from rain areas with similar sizes. In Fig. 11a, the distribution of total counts of thresholds across *O*/*N* is plotted, and the larger events toward A+ are more capable to produce rain areas larger in size (say, ≥60% of Taiwan). Also, the counts remain mostly around 50 for *O*/*N* ≥ 40%, then rise to 200-300 with *O*/*N* ≤ 10%.

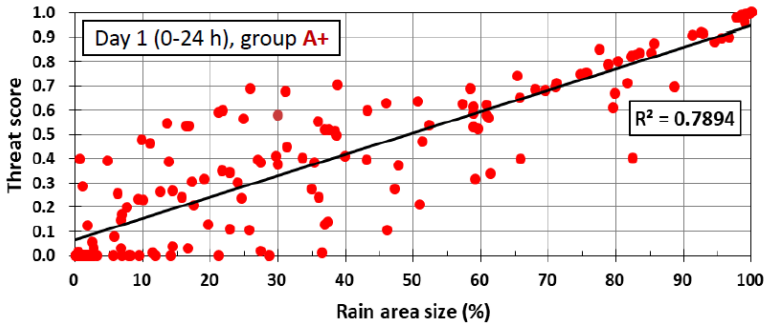

Figure 10: Scatter plot of TS versus observed rain-area size (%) from day-1 QPFs for group A+ from 0% to 100% (from high to low rainfall threshold). The square of correlation coefficient (R^2) is given.

Due to fewer samples at larger *O*/*N* values, the TSs for different groups (from a single 2 × 2 table for each bin) are presented only for *O*/*N* ≤ 40% in Figs. 11b-d. While the scores for B-D are roughly the same, the TSs for A are clearly higher compared to them on day 1, and those for A+ are again higher compared to A on days 1 and 2 over most part of this range, sometimes by 0.05-0.1, when the factor of rain-area size is removed (Figs. 11b,c). On day 3 (Fig. 11d), however, the TSs for larger events (A+ and A) show no particular advantage. Therefore, similar to typhoons in W15, the 2.5-km CReSS is more skillful in predicting the larger mei-yu events in Taiwan within 2 days, over the heavy-rainfall area (again, mainly over the mountains).

The higher TSs and better skill for large events at *O*/*N* within 40% (Fig. 11) are most likely linked to the more favorable conditions at synoptic to meso-α scale, which the model is capable to capture with higher accuracy (e.g., Walser and Schär, 2004). To briefly elaborate on this aspect, seven items on the checklist used by CWB forecasters in the mei-yu season as a guidance to issue heavy-rainfall warning (e.g., Wang et al., 2012a) are selected, and their occurrence frequency, judged using surface weather maps and NCEP gridded analyses at the starting time of each 24-h periods are compiled for different groups. These items include: 1) presence of surface mei-yu front inside 20°-28°N, 118°-124°E; 2) Taipei (cf. Fig. 3) within 200 km south and 100 km north of the front; 3) Kaoshiung (cf. Fig. 3) within 200 km south of the front; 4) presence of low-level jet (LLJ) inside 18°-26°N, 115°-125°E at 850 or 700 hPa; 5) presence of mesolow near Taiwan; 6) Taiwan inside a low pressure zone; and 7) the mean sea-level pressure in Taiwan is below 1005 hPa. The results (Fig. 12) indicate that among the seven items, an average of 4.15 items are met in group A+, and this figure gradually declines toward smaller groups, from 3.67 in A, 2.84 in B, and finally to only 0.87 in X.

Thus, as expected, the synoptic and meso-α-scale conditions tend to be more favorable in larger events. Such conditions, in combination with orographic forcing in Taiwan, appear to allow for better model performance in QPFs, given a sufficient resolution.

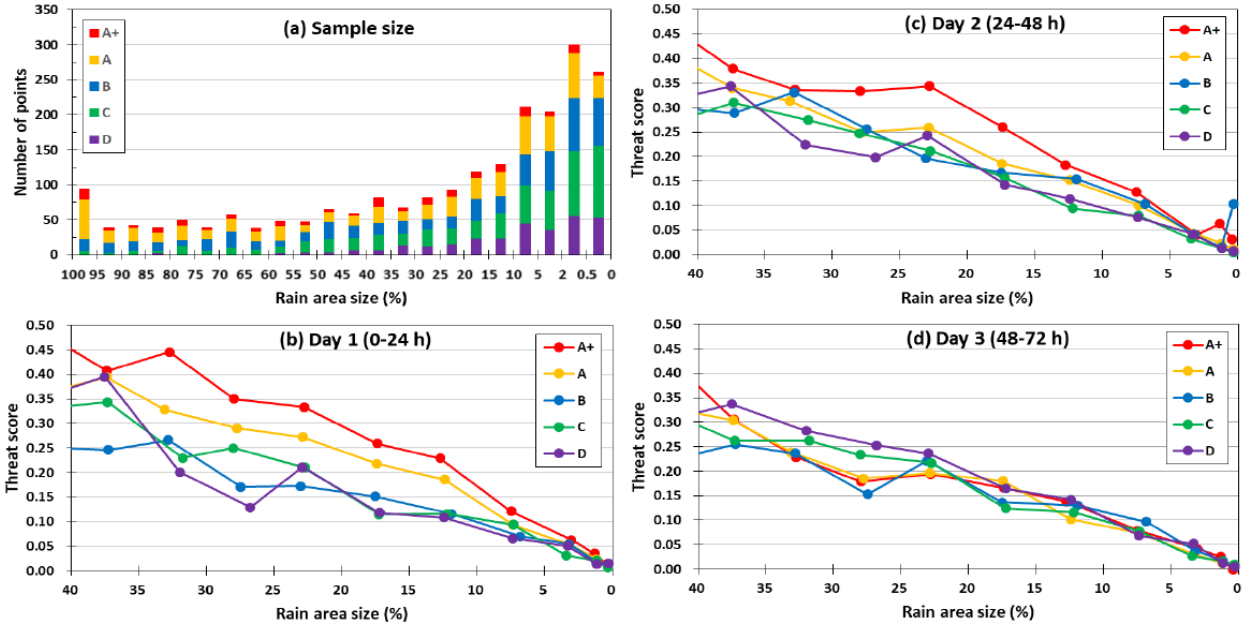

Figure 11: (a) The distribution of data points in the bins of observed rain-area size (%, every 5% from 100% to 5%, then 2-5%, 0.5-2%, and < 0.5%; same for days 1-3) among groups A+ and A to D. (b)-(d) The TS of 24-h QPFs for (b) day 1 to (d) day 3, respectively, as a function of observed rain-area size between 40% and 0%.

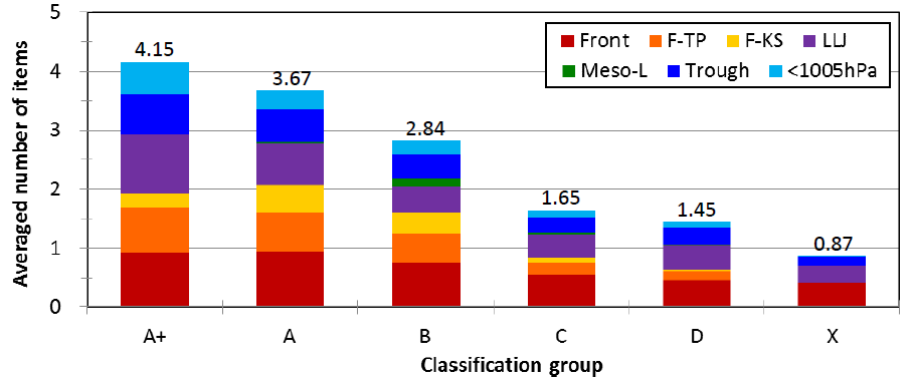

Figure 12: The average number of items met, among the seven items on the checklist, at the starting time of 24-h segments for different classification groups (from A+, A to D, and X), with the value labeled on top. Following the order (bottom to top), the seven items are: presence of surface mei-yu front (front), front near Taipei (F-TP), front near Kaoshiung (F-KS), presence of LLJ, mesolow (meso-L), Taiwan inside a low pressure zone (trough), and the mean sea-level pressure lower than 1005 hPa (<1005 hPa), respectively. The items are plotted in different colors (see insert) to show their proportion.

6 Summary and Concluding Remarks

In this study, the QPFs at the ranges of 1-3 days by the 2.5-km CReSS during three mei-yu seasons (May-June) in Taiwan of 2012-2014 are evaluated using categorical statistics, with an emphasis on heavy to extreme rainfall events (100-500 mm per 24 h). In this section, our results are briefly summarized and the concluding remarks are given.

Overall, the TSs of day-1 QPFs for all events (no classification) at thresholds of 100, 250, and 500 mm are 0.18, 0.15 and 0.09, respectively. Compared to previous and contemporary results from models at lower resolutions for mei-yu season in Taiwan (Section 1, e.g., Hsu et al., 2014; Li and Hong, 2014; Su et al., 2016; Huang et al., 2016), the results herein show significant improvements by the 2.5-km CReSS, especially over the heavy-rainfall thresholds.

Moreover, when proper classification based on observed rain-area size (i.e., event magnitude) are used, the CRM's ability to predict the extreme and top events (group A+) in terms of the TS are much higher. For the top 4% and most hazardous mei-yu events, the day-1 QPFs have TSs of 0.34, 0.24, and 0.16, respectively, at the same thresholds. The QPFs for larger events also exhbit higher POD, lower FAR, and higher TS than smaller ones, across nearly all thresholds at all ranges of days 1-3. Thus, the positive dependency in categorical scores on the overall rainfall amount also exists in mei-yu regime in Taiwan, as predicted by W15 (and Wang, 2016).

Through further analysis of example case, the improvement by the 2.5-km CReSS in Taiwan is shown to lie in an improved ability to capture the phase-locked topographic rainfall at its correct location in larger events at heavy-rainfall thresholds. For stationary rainfall in the mountains, the QPFs tend to be more accurate as the CRM can better resolve both the terrain and convection (e.g., also Walser and Schär, 2004; Roberts and Lean, 2007). In contrast, the concentrated rainfall caused by transient systems (such as frontal squall lines) is highly random and more difficult to predict at the correct time and location due to nonlinearity, even though a realistic scenario is produced and the potential of heavy rainfall indicated (unless at short-enough ranges). For such rainfall, model QPFs are still informative and useful, but the categorical statistics may not be. Overall, the high-resolution models may possess a higher QPF skill in categorical statics for extreme events than ordinary ones, at least for regions like Taiwan as demonstrated here (and in W15). Such QPFs can be helpful to hazard preparation and mitigation.

Code and data availability

The model used in this study is called Cloud-Resloving Storm Simulator and its website for downloading model and user's guide is at http://www.rain.hyarc.nagoya-u.ac.jp/~tsuboki/cress_html/index_cress_eng.html. And the rainfall figures of Model is at the website http://cressfcst.es.ntnu.edu.tw/.

Author contribution

Chung-Chieh Wang designed the experiments and Pi-Yu Chuang carried them out. Chih-Sheng Chang operated the real-time model forecasting and Kazuhisa Tsuboki created the model code. Shin-Yi Huang helped with some figures and Guo-Chen Leu provided some CWB results. Chung-Chieh Wang prepared the manuscript with contributions from all co-authors.

Competing interests

The authors declare that they have no conflict of interest.

Acknowledgments

Constructive comments and suggestions from two anonymous reviewers and Prof. George Tai-Jen Chen of the National Taiwan University are appreciated. The first author, CCW, wishes to thanks assistants Ms. Y.-W. Wang, Mr. T.-C. Lin, and Mr. K.-Y. Chen for their help on this study. The CWB is acknowledged for providing the observational data, the radar plots, and the QPF verification results in Fig. 2. The National Center for High-performance Computing (NCHC) and the Taiwan Typhoon and Flood Research Institute (TTFRI) provided the computational resources. This study is jointly supported by the Ministry of Science and Technology of Taiwan under Grants MOST-103-2625-M-003-001-MY2, MOST-105-2111-M-003-003-MY3, MOST-108-2111-M-003-005-MY2, MOST-110-2111-M-003-004, and MOST-110-2625-M-003-001.

References

Barnes, L. R., Schultz, D. M., Gruntfest, E. C., Hayden, M. H., and Benight, C. C.: Corrigendum: False alarm rate or false alarm ratio?, Weather Forecast., 24, 1452–1454, https://doi.org/10.1175/2009WAF2222300.1, 2009.

Bryan, G. H., Wyngaard, J. C., and Fritsch, J. M.: Resolution requirements for the simulation of deep moist convection, Mon. Weather Rev., 131, 2394–2416, https://doi.org/10.1175/1520-0493(2003)131%3C2394:RRFTSO%3E2.0.CO;2, 2003.

Chang, C.-P., Yeh, T.-C., and Chen, J.-M.: Effects of terrain on the surface structure of typhoons over Taiwan, Mon. Weather Rev., 121, 734–752, https://doi.org/10.1175/1520-0493(1993)121%3C0734:EOTOTS%3E2.0.CO;2, 1993.

Chang, C.-P., Yang, Y.-T., and Kuo, H.-C.: Large increasing trend of tropical cyclone rainfall in Taiwan and the roles of terrain, J. Clim., 26, 4138–4147, https://doi.org/10.1175/JCLI-D-12-00463.1, 2013.

Chen, C.-S., and Chen, Y.-L.: The rainfall characteristics of Taiwan. Mon. Weather Rev., 131, 1324–1341, 2003.

Chen, G. T.-J., Wang, C-C., and Lin, D. T.-W.: Characteristics of low-level jets over northern Taiwan in Mei-yu season and their relationship to heavy rain events, Mon. Weather Rev., 133, 20–43, https://doi.org/10.1175/MWR-2813.1, 2005.

Chen, T.-C., Yen, M.-C., Hsieh, J.-C., and Arritt, R. W.: Diurnal and seasonal variations of the rainfall measured by the Automatic Rainfall and Meteorological Telemetry System in Taiwan. Bull. Amer. Meteor. Soc., 80, 2299–2312, doi:10.1175/1520-0477(1999)080,2299: DASVOT.2.0.CO;2, 1999.

Cheung, K. K. W., Huang, L.-R., and Lee, C.-S.: Characteristics of rainfall during tropical cyclone periods in Taiwan, Nat. Hazards Earth Syst. Sci., 8, 1463–1474, https://doi.org/10.5194/nhess-8-1463-2008, 2008.

Chi, S.-S.: The Mei-Yu in Taiwan, SFRDEST E-06-MT-03-4, Chung-Shin Engineering Technology Research and Development Foundation, Taipei, Taiwan, 65 pp, 2006. (in Chinese)

Chien, F.-C., and Jou, B. J.-D.: MM5 ensemble mean precipitation in the Taiwan area for three early summer convective (Mei-Yu) seasons, Weather Forecast., 19, 735–750, 2004.

Chien, F.-C., Kuo, Y.-H., and Yang, M.-J.: Precipitation forecast of MM5 in the Taiwan area during the 1998 Mei-yu season, Weather Forecast., 17, 739–754, https://doi.org/10.1175/1520-0434(2002)017%3C0739:PFOMIT%3E2.0.CO;2, 2002.

Chien, F.-C., Liu, Y.-C., and Jou, B. J.-D.: MM5 ensemble mean forecasts in the Taiwan area for the 2003 Mei-yu season, Weather Forecast., 21, 1006–1023, https://doi.org/10.1175/WAF960.1, 2006.

Clark, A. J., Gallus, Jr., W. A., and Chen, T.-C.: Comparison of the diurnal precipitation cycle in convection-resolving and non-convection-resolving mesoscale models, Mon. Weather Rev., 135, 3456–3473, https://doi.org/10.1175/MWR3467.1, 2007.

Clark, A. J., Kain, J. S., Stensrud, D. J., Xue, M., Kong, F., Coniglio, M. C., Thomas, K. W., Wang, Y., Brewster, K., Gao, J., Wang, X., Weiss, S. J., and Du, J.: Probabilistic precipitation forecast skill as a function of ensemble size and spatial scale in a convection-allowing ensemble, Mon. Weather Rev., 139, 1410–1418, https://doi.org/10.1175/2010MWR3624.1, 2011.

Cotton, W. R., Tripoli, G. J., Rauber, R. M., and Mulvihill, E. A.: Numerical simulation of the effects of varying ice crystal nucleation rates and aggregation processes on orographic snowfall, J. Appl. Meteorol. Climatol., 25, 1658–1680, https://doi.org/10.1175/1520-0450(1986)025%3C1658:NSOTEO%3E2.0.CO;2, 1986.

Cuo, L., Pagano, T. C., and Wang, Q. J.: A review of quantitative precipitation forecasts and their use in short- to medium-range streamflow forecasting, J. Hydormeteorol., 12, 713–728, https://doi.org/10.1175/2011JHM1347.1, 2011.

Davis, C., Brown, B., and Bullock, R.: Object-based verification of precipitation forecasts. Part I: Methodology and application to mesoscale rain areas, Mon. Weather Rev., 134, 1772–1784, https://doi.org/10.1175/MWR3145.1, 2006.

Deardorff, J. W.,: Stratocumulus-capped mixed layers derived from a three-dimensional model, Bound.-Layer Meteorol., 18, 495–527, 1980.

Done, J., Davis, C. A., and Weisman, M.: The next generation of NWP: explicit forecasts of convection using the weather research and forecasting (WRF) model, *Atmos. Sci. Lett.*, *5*, 110–117, 2004.

Ebert, E. E.: Ability of a poor man's ensemble to predict the probability and distribution of precipitation, Mon. Weather Rev., 129, 2461–2480, https://doi.org/10.1175/1520-0493(2001)129%3C2461:AOAPMS%3E2.0.CO;2, 2001.

Ebert, E. E., and McBride, J. L.: Verification of precipitation in weather systems: Determination of systematic errors, J. Hydrol., 239, 179–202, https://doi.org/10.1016/S0022-1694(00)00343-7, 2000.

Ebert, E. E., Damrath, U., Wergen, W., and Baldwin, M. E.: The WGNE assessment of short-term quantitative precipitation forecasts (QPFs) from operational numerical weather prediction models, Bull. Am. Meteorol. Soc., 84, 481–492, https://doi.org/10.1175/BAMS-84-4-481, 2003.

Fang, X., and Kuo, Y.-H.: Improving ensemble-based quantitative precipitation forecasts for topography-enhanced typhoon heavy rainfall over Taiwan with a modified probability-matching technique, Mon. Weather Rev., 141, 3908–3932, https://doi.org/10.1175/MWR-D-13-00012.1, 2013.

Fritsch, J. M., and Carbone, R. E.: Improving quantitative precipitation forecasts in the warm season. A USWRP research and development strategy, Bull. Am. Meteorol. Soc., 85, 955–965, https://doi.org/10.1175/BAMS-85-7-955, 2004.

Gilleland, E., Ahijevych, D. A., Brown, B. G., and Ebert, E. E.: Verifying forecasts spatially, Bull. Am. Meteorol. Soc., 91, 1365–1373, https://doi.org/10.1175/2010BAMS2819.1, 2010.

Golding, B. W.: Quantitative precipitation forecasting in the UK. J. Hydrol., 239, 286–305, https://doi.org/10.1016/S0022-1694(00)00354-1, 2000.

Hochman, A., Scher, S., Quinting, J., Pinto, J. G., and Messori, G.: A new view of heat wave dynamics and predictability over the eastern Mediterranean, Earth Syst. Dynam., 12, 133–149, https://doi.org/10.5194/esd-12-133-2021, 2021.

Hong, J.-S.: Evaluation of the high-resolution model forecasts over the Taiwan area during GIMEX, Weather and Forecast., 18, 836–846, https://doi.org/10.1175/1520-0434(2003)018%3C0836:EOTHMF%3E2.0.CO;2, 2003.

Hong, J.-S., Fong, C.-T., Hsiao, L.-F., Yu, Y.-C., and Tseng, C.-Y.: Ensemble typhoon quantitative precipitation forecasts model in Taiwan, Weather Forecast., 30, 217–237, https://doi.org/10.1175/WAF-D-14-00037.1, 2015.

Hsu, J.: ARMTS up and running in Taiwan, Väisälä News, 146, 24–26, 1998.

Hsu, J. C.-S., Wang, C.-J., Chen, P.-Y., Chang, T.-H., and Fong, C.-T. (2014), Verification of quantitative precipitation forecasts by the CWB WRF and ECMWF on 0.125° grid, in: Proceedings of 2014 Conference on Weather Analysis and Forecasting, Central Weather Bureau, Taipei, Taiwan, 16-18 September 2014, A2-24, 2014. (in Chinese)

Huang, T.-S., Yeh, S.-H., Leu, G.-C., and Hong, J.-S.:, A synthesis and comparison of QPF verifications at the CWB and major NWP guidance, in: Proceedings of 2015 Conference on Weather Analysis and Forecasting, Central Weather Bureau, Taipei, Taiwan, 15-17 September 2015, A7-11, 2015. (in Chinese)

Huang, T.-S., Yeh, S.-H., Leu, G.-C., and Hong, J.-S.: Postprocessing of ensemble rainfall forecasts---Ensemble mean, probability matched mean and exceeding probability, Atmospheric Sciences, 44, 173–196, 2016. (in Chinese with English abstract)

Ikawa, M., and Saito, K: Description of a non-hydrostatic model developed at the Forecast Research Department of the MRI, Technical Report, 28, Meteorological Research Institute, Tsukuba, Ibaraki, Japan, 245 pp, 1991.

Jou, B. J.-D., Lee, W.-C., and Johnson, R. H.: An overview of SoWMEX/TiMREX, in: The Global Monsoon System: Research and Forecast, 2nd Edition, edited by: Chang, C.-P., Ding, Y., Lau, N.-C., Johnson, R. H., Wang, B., Yasunari, T., World Scientific, Toh Tuck Link, Singapore, 303–318, https://doi.org/10.1142/9789814343411_0018, 2011.

Kalnay, E., Kanamitsu, M., and Baker, W. E.: Global numerical weather prediction at the National Meteorological Center, Bull. Am. Meteorol. Soc., 71, 1410–1428, 1990.

Kanamitsu, M.: Description of the NMC global data assimilation and forecast system, Weather Forecast., 4, 335–342, https://doi.org/10.1175/1520-0434(1989)004%3C0335:DOTNGD%3E2.0.CO;2, 1989.

Kleist, D. T., Parrish, D. F., Derber, J. C., Treadon, R., Wu, W. S., and Lord, S.: Introduction of the GSI into the NCEP global data assimilation system, Weather Forecast., 24, 1691–1705, https://doi.org/10.1175/2009WAF2222201.1, 2009.

Kondo, J.: Heat balance of the China Sea during the air mass transformation experiment, J. Meteor. Soc. Japan, 54, 382–398, https://doi.org/10.2151/jmsj1965.54.6_382, 1976.

Kuo, Y.-H., and Chen, G. T.-J.: The Taiwan Area Mesoscale Experiment (TAMEX): An overview, Bull. Am. Meteorol. Soc., 71, 488–503, http://dx.doi.org/10.1175/1520-0477(1990)071%3C0488:TTAMEA%3E2.0.CO;2, 1990.

Li, C.-H., and Hong, J.-S.: Study on the application and analysis of regional ensemble quantitative precipitation forecasts, in: Proceedings of 2014 Conference on Weather Analysis and Forecasting, Central Weather Bureau, Taipei, Taiwan, 16-18 September 2014, A2-19, 2014. (in Chinese)

Li, J. and Chen, Y.-L.: Barrier jets during TAMEX, Mon. Weather Rev., 126, 959–971, https://doi.org/10.1175/1520-0493(1998)126%3C0959:BJDT%3E2.0.CO;2, 1998.

Lin, Y.-L., Farley, R. D., and Orville, H. D.: Bulk parameterization of the snow field in a cloud model, J. Appl. Meteorol. Climatol., 22, 1065–1092, https://doi.org/10.1175/1520-0450(1983)022%3C1065:BPOTSF%3E2.0.CO;2, 1983.

Louis, J. F., Tiedtke, M., and Geleyn, J. F.: A short history of the operational PBL parameterization at ECMWF, in: Proceedings of Workshop on Planetary Boundary Layer Parameterization, Shinfield Park, Reading, UK, 25-27 November 1981, 59–79, 1982.

Moorthi, S., Pan, H. L., and Caplan, P.: Changes to the 2001 NCEP operational MRF/AVN global analysis/forecast system, NWS Technical Procedures Bulletin, 484, Office of Meteorology, National Weather Service, Silver Spring, Maryland, USA, 2001.

Murakami, M.: Numerical modeling of dynamical and microphysical evolution of an isolated convective cloud---The 19 July 1981 CCOPE cloud, J. Meteor. Soc. Japan, 68, 107–128, https://doi.org/10.2151/jmsj1965.68.2_107, 1990.

Murakami, M., Clark, T. L., and Hall, W. D.: Numerical simulations of convective snow clouds over the Sea of Japan: Two-dimensional simulation of mixed layer development and convective snow cloud formation, J. Meteor. Soc. Japan, 72, 43–62, https://doi.org/10.2151/jmsj1965.72.1_43, 1994.

Paul, S., Wang, C.-C., Chien, F.-C., and Lee, D.-I.: An evaluation of the WRF Mei-yu rainfall forecasts in Taiwan, 2008-2010: differences in elevation and sub-regions. Meteorol. Appl., 25, 269-282, doi: 10.1002/met.1689, 2018.

Roberts, N. M., and Lean, H. W.: Scale-selective verification of rainfall accumulations from high-resolution forecasts of convective events, Mon. Weather Rev., 136, 78–97, https://doi.org/10.1175/2007MWR2123.1, 2007.

Roebber, P. J.: Visualizing multiple measures of forecast quality, Weather Forecast., 24, 601–608, https://doi.org/10.1175/2008WAF2222159.1, 2009.

Schaefer, J. T.: The critical success index as an indicator of warning skill, Weather Forecast., 5, 570–575, https://doi.org/10.1175/1520-0434(1990)005%3C0570:TCSIAA%3E2.0.CO;2, 1990.

Segami, A., Kurihara, K., Nakamura, H., Ueno, M., Takano, I., and Tatsumi, Y.: Operational mesoscale weather prediction with Japan Spectral Model, J. Meteor. Soc. Japan, 67, 907–924, https://doi.org/10.2151/jmsj1965.67.5_907, 1989.

Skamarock, W. C., Klemp, J. B., Dudhia, J., Gill, D. O., Barker, D. M., Wang, W., and Powers, J. G.: A description of the advanced research WRF version 2, National Center for Atmospheric Reasearch, Boulder, Colorado, USA, 88 pp, http://dx.doi.org/10.5065/D6DZ069T, 2005.

Su, Y.-J., Hong, J.-S., and Li, C.-H.: The characteristics of the probability matched mean QPF for 2014 Meiyu season, Atmospheric Sciences, 44, 113-134, 2016. (in Chinese with English abstract)

Tsuboki, K., and Sakakibara, A.: Large-scale parallel computing of cloud resolving storm simulator, in: High Performance Computing, edited by: Zima H. P., Joe K., Sato M., Seo Y., Shimasaki M., Springer, Berlin, Heidelberg, Germany, 243–259, https://doi.org/10.1007/3-540-47847-7_21, 2002.

Tsuboki, K., and Sakakibara, A.: Numerical Prediction of High-Impact Weather Systems: The Textbook for the Seventeenth IHP Training Course in 2007, Hydrospheric Atmospheric Research Center, Nagoya University, Nagoya, Japan, and UNESCO, Paris, France, 273 pp, 2007.

Walser, A., and Schär, C.: Convection-resolving precipitation forecasting and its predictability in Alpine river catchments, J. Hydrol., 288, 57–73, https://doi.org/10.1016/j.jhydrol.2003.11.035, 2004.

Wang, C.-C.: On the calculation and correction of equitable threat score for model quantitative precipitation forecasts for small verification areas: The example of Taiwan, Weather Forecast., 29, 788–798, https://doi.org/10.1175/WAF-D-13-00087.1, 2014.

Wang, C.-C.: The more rain, the better the model performs—The dependency of quantitative precipitation forecast skill on rainfall amount for typhoons in Taiwan, Mon. Weather Rev., 143, 1723–1748, https://doi.org/10.1175/MWR-D-14-00137.1, 2015.

Wang, C.-C.: News and notes, Paper of notes: The more rain from typhoons, the better the models perform, Bull. Am. Meteorol. Soc., 97, 16–17, https://doi.org/10.1175/BAMS_971_11-18_Nowcast, 2016.

Wang, C.-C., Chen, G. T.-J., Chen, T.-C., and Tsuboki, K.: A numerical study on the effects of Taiwan topography on a convective line during the mei-yu season, Mon. Weather Rev., 133, 3217–3242, https://doi.org/10.1175/MWR3028.1, 2005.

Wang, C.-C., Chen, G. T.-J., and Huang, S.-Y.: Remote trigger of deep convection by cold outflow over the Taiwan Strait in the Mei-yu season: A modeling study of the 8 June 2007 Case, Mon. Weather Rev., 139, 2854–2875, https://doi.org/10.1175/2011MWR3613.1, 2011.

Wang, C.-C., Kung, C.-Y., Lee, C.-S., and Chen, G. T.-J.: Development and evaluation of Mei-yu season quantitative precipitation forecast in Taiwan river basins based on a conceptual climatology model, Weather Forecast., 27, 586–607, https://doi.org/10.1175/WAF-D-11-00098.1, 2012a.

Wang, C.-C., Kuo, H.-C., Chen, Y.-H., Huang, H.-L., Chung, C.-H., and Tsuboki, K.: Effects of asymmetric latent heating on typhoon movement crossing Taiwan: The case of Morakot (2009) with extreme rainfall, J. Atmos. Sci., 69, 3172–3196, https://doi.org/10.1175/JAS-D-11-0346.1, 2012b.

Wang, C.-C., Chen, Y.-H., Kuo, H.-C., and Huang, S.-Y.: Sensitivity of typhoon track to asymmetric latent heating/rainfall induced by Taiwan topography: A numerical study of Typhoon Fanapi (2010), J. Geophys. Res. Atmos., 118, 3292–3308, https://doi.org/10.1002/jgrd.50351, 2013a.

Wang, C.-C., Kuo, H.-C., Yeh, T.-C., Chung, C.-H., Chen, Y.-H., Huang, S.-Y., Wang, Y.-W., and Liu, C.-H.: High-resolution quantitative precipitation forecasts and simulations by the Cloud-Resolving Storm Simulator (CReSS) for Typhoon Morakot (2009), J. Hydrol., 506, 26–41. https://doi.org/10.1016/j.jhydrol.2013.02.018, 2013b.

Wang, C.-C., Huang, S.-Y., Chen, S.-H., Chang, C.-S., and Tsuboki, K.: Cloud-resolving typhoon rainfall ensemble forecasts for Taiwan with large domain and extended range through time-lagged approach, Weather Forecast., 31, 151–172, https://doi.org/10.1175/WAF-D-15-0045.1, 2016a.

Wang, C.-C., Chiou, B.-K., Chen, G. T.-J., Kuo, H.-C., and Liu, C.-H.: A numerical study of back-building process in a quasistationary rainband with extreme rainfall over northern Taiwan during 11-12 June 2012, Atmos. Chem. Phys., 16, 12359–12382, https://doi.org/10.5194/acp-16-12359-2016, 2016b.

Wang, C.-C., Paul, S., Chien, F.-C., Lee, D.-I., and Chuang, P.-Y.: An evaluation of WRF rainfall forecasts in Taiwan during three mei-yu seasons of 2008-2010, Weather Forecast., 32, 1329–1351, https://doi.org/10.1175/WAF-D-16-0190.1, 2017.

Wernli, H., Paulat, M., Hagen, M., and Frei, C.: SAL—A novel quality measure for the verification of quantitative precipitation forecasts, Mon. Weather Rev., 136, 4470–4487, https://doi.org/10.1175/2008MWR2415.1, 2008.

Wilks, D. S.: Statistical methods in the atmospheric sciences, 3rd Edition. Academic Press, San Diego, California, USA, 2011.

Wu, C.-C., and Kuo, Y.-H.: Typhoons affecting Taiwan: Current understanding and future challenges, Bull. Am. Meteorol. Soc., 80, 67–80, https://doi.org/10.1175/1520-0477(1999)080%3C0067:TATCUA%3E2.0.CO;2, 1999.

Yang, M.-J., Jou, B. J.-D., Wang, S.-C., Hong, J.-S., Lin, P.-L., Teng, J.-H., and Lin, H.-C.: Ensemble prediction of rainfall during the 2000–2002 mei-yu seasons: Evaluation over the Taiwan area, J. Geophys. Res., 109, D18203, https://doi.org/10.1029/2003JD004368, 2004.

Yeh, H.-C., and Chen, Y.-L.: Characteristics of the rainfall distribution over Taiwan during TAMEX, J. Appl. Meteorol. Climatol., 37, 1457–1469, https://doi.org/10.1175/1520-0450(1998)037%3C1457:CORDOT%3E2.0.CO;2, 1998.

Yeh, H.-C., and Chen, Y.-L.: The role of off shore convergence on coastal rainfall during TAMEX IOP 3, Mon. Weather Rev., 130, 2709–2730, https://doi.org/10.1175/1520-0493(2002)130%3C2709:TROOCO%3E2.0.CO;2, 2002.